SEEING IN THE LIGHT: USING EXPANSION MICROSCOPY TO ACHIEVE SUPER-RESOLUTION IN TRANSMITTED LIGHT

Julia R. Migliore

Thesis Prepared for the Degree of

MASTER OF SCIENCE

UNIVERSITY OF NORTH TEXAS

December 2022

APPROVED:

Douglas Root, Major Professor
Kent Chapman, Committee Member
Rebecca Dickstein, Committee Member
Jyoti Shah, Chair of the Department of Biological Sciences
John Quintanilla, Interim Dean of the College of Science
Victor Prybutok, Dean of the Toulouse Graduate School

Migliore, Julia R. *Seeing in the Light: Using Expansion Microscopy to Achieve Super-Resolution in Transmitted Light*. Master of Science (Biochemistry and Molecular Biology), December 2022, 60 pp., 26 figures, reference list, 35 titles.

Light microscopy is inherently limited in resolution by properties of light such as diffraction and interference to 170-250 nm. Expansion microscopy is a quickly-developing method which achieves super-resolution by using a swellable hydrogel to physically expand biological samples themselves, rather than depending on the properties of fluorophores. This thesis demonstrates that expansion microscopy is a feasible means for achieving super-resolution in transmitted light microscopy modes. Though it has only been used for fluorescence imaging in the past, here I show that samples prepared for expansion microscopy—including liver tissue slices and myofibrillar bundles—are observable using transmitted light. While the majority of the original sample material is removed in the expansion process, the hydrogel retains visible evidence of these samples. These demonstrate increased detail under brightfield microscopy that is useful for characterization. Sarcomeric regions are identifiable by this method and are confirmed by fluorescence imaging. Thus, expansion microscopy is a means to bring super-resolution to transmitted light imaging and is entirely compatible with fluorescence for the localization of proteins of interest.

ACKNOWLEDGEMENTS

I could not have accomplished the work described in this thesis without the support of so many others, both inside and outside of the lab. Many thanks to Dr. Douglas Root, my major professor and P.I., for his continued feedback regarding all elements of the research and writing of this work. Likewise, I'd like to recognize my committee members, both current (Dr. Rebecca Dickstein and Dr. Kent Chapman) and former (Dr. Mauricio Antunes and Dr. Pamela Padilla), for facilitating all of the necessary milestones of my degree, including the review of this thesis.

I could not have undertaken this work without Dr. Andrea Bernadino-Schaefer, who has greatly invested in my training as a microscopist. I am also so grateful for my lab-mates, Dr. Motamed Qadan and Dua'a Quedan, for helping me get to know our lab with all kindness and patience.

Of course, none of this research would have been possible without funding from the National Institutes of Health via NIH/NHLBI R01HL149164.

I would also like to acknowledge my husband, Andre Migliore, for his support of my scholarly goals in every way as well as my sweet child Benjamin, who has pushed me to evaluate the impact of everything I do, including research. This thesis is for you.

Lastly and above all, I thank God for his sovereignty and his goodness. I have accomplished this work at this time and in this place because he willed it to be so. He created my mind, the ability to reason, all of the incredible things there are in this world to study (muscles included, of course), and the means to communicate what I have uncovered. May this thesis highlight his glory as seen in the natural world and his grace in letting me get to know a piece of it.

TABLE OF CONTENTS

Page

LIST OF FIGURES

LIST OF ABBREVIATIONS

A band	Anisotropic band
ANOVA	Analysis of variance
AP	Alkaline phosphatase
APS	Ammonium persulfate
BCIP/NBT	Nitro-blue tetrazolium chloride/5-bromo-4-chloro-3'-indolyphosphate p-toluidine
C	Celsius
C-Apo	C-apochromat
cm	Centimeter
DAPI	4′,6-Diamidino-2-phenylindole
DIC	Differential interference contrast
DNA-PAINT	Deoxyribonucleic acid-point accumulation in nanoscale topology
dSTORM	Direct stochastic optical reconstruction microscopy
EDTA	Ethylenediaminetetraacetic acid
EMCCD	Electron-multiplying charge-coupled device
ExM	Expansion microscopy
FITC	Fluorescein isothiocyanate
g	Gram
GFP	Green fluorescent protein
HCl	Hydrochloric acid
I band	Isotropic band
IHC	Immunohistochemistry/immunohistochemical
L	Liter

M	Molar
MAP	Magnified analysis of the proteome
mg	Milligram
mL	Milliliter
MyBPC	Myosin-binding protein C
MyBPH	Myosin-binding protein H
MyBPHL	Myosin-binding protein H-like
NA	Numerical aperture
NaCl	Sodium chloride
nm	Nanometer
NSOM	Near field scanning microscopy
O.C.T.	Optimal cutting temperature
p	Probability value
PALM	Photoactivated localization microscopy
PBS	Phosphate-buffered saline
PlanApo	Plan apochromat
pro-ExM	Protein retention expansion microscopy
r	Correlation coefficient
RNA	Ribonucleic acid
SDS	Sodium dodecyl sulfate
SIM	Structured illumination microscopy
SL	Sarcomere length
STED	Stimulated emission depletion

TAMRA	5-Carboxytetramethylrhodamine
TEMED	Tetramethylethylenediamine
TEMPO	2,2,6,6-Tetramethylpiperidinyloxy
TRITC	Tetramethylrhodamine isothiocyanate
xg	Multiple of the gravitational constant
µM	Micromolar
µm	Micron

CHAPTER 1

INTRODUCTION

1.1 The Sarcomere

Muscle contraction can be attributed to the concerted action of sarcomeres, highly organized complexes of proteins. A single myocyte contains many sarcomeres, organized into units called “myofibrils.” The basis of the sarcomere consists of interdigitating myosin filaments and actin filaments, with two mirrored myosin filaments attached and aligned by structural proteins at the M-line (Figure 1.1-1) (Lange et al., 2005). The edges of the sarcomere are defined by the Z-discs, which attach and align actin filaments (Takahashi & Hattori, 1989).

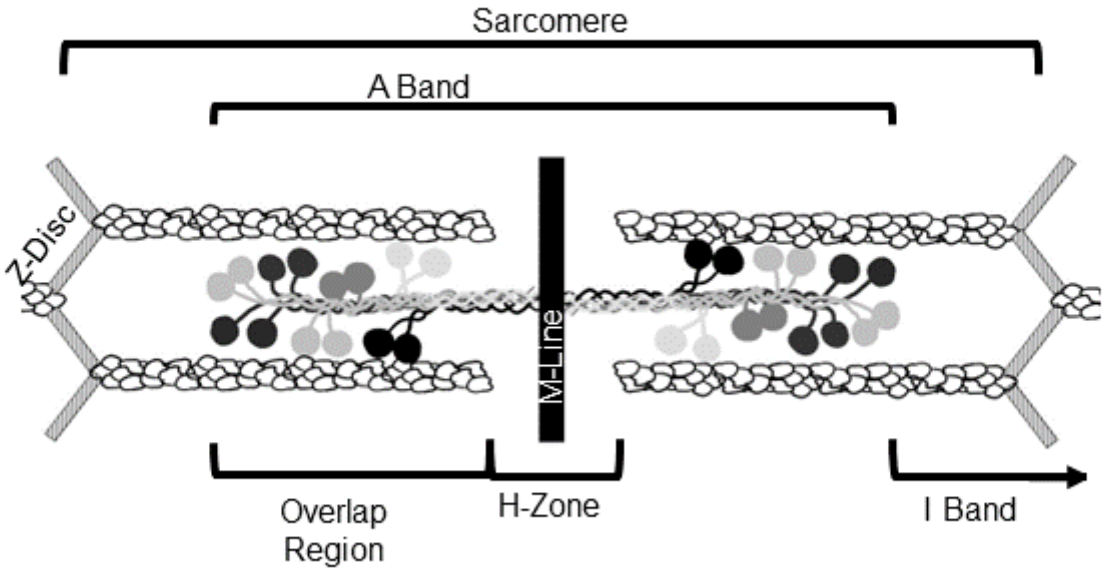

Figure 1.1-1. Sarcomere Structure

Changes in the sarcomere during contraction were first described in 1954 (A. F. Huxley & Niedergerke, 1954; H. Huxley & Hanson, 1954). Huxley and colleagues observed two alternating striations with interference microscopy, the anisotropic (A)

band and the isotropic (I) band. The A band's width remains constant throughout contraction and relaxation, while the I band's width changes. This observation was explained upon recognizing the A band as the myosin filaments, which remain in place throughout contraction. The I band is defined as the portion of actin filaments which does not overlap with myosin. Therefore, as the sarcomere shortens and filaments overlap more, the I band decreases in width (Figure 1.1-2). Similarly, the portion of myosin filaments which does not overlap with actin (called the "H zone") decreases in width with contraction (Aronson, 1967).

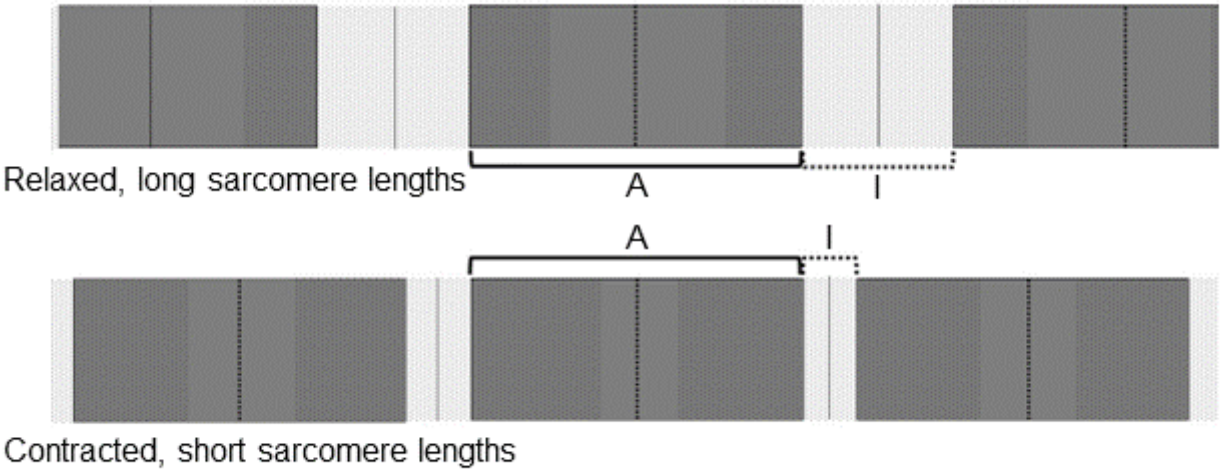

Figure 1.1-2. Changes in Sarcomeric Features upon Contraction

Observations of the changing sarcomere and the accumulation of more structural data eventually lead to the swinging crossbridge model of contraction, which posited that during contraction, the heads of myosin proteins bind actin and pull actin filaments towards the M-line (H. E. Huxley, 1969). This increases the overlap of myosin and actin, resulting in sarcomere shortening. Thus, the micro-scale shortening of many sarcomeres results in the large-scale shortening or contraction of a muscle.

The binding and motor functions of myosin are activated by calcium signaling via troponins and tropomyosin and regulated by post-translational modifications via several sarcomeric proteins. The details of contraction regulation are beyond the scope of this work but are reviewed in the following (Brown & Cohen, 2005; Heling et al., 2020; Ito et al., 2021; Schmid & Toepfer, 2021). Nevertheless, it is often important to note the locations of these proteins in the sarcomere. Tropomyosin twists around the full length of the actin thin filament. Troponin complexes also decorate the thin filament, every 27.5-Å (Paul et al., 2009). Myosin binding protein C (MyBPC) and related myosin binding proteins H and H-like (MyBPH and MyBPHL) are tethered to the myosin thick filament in areas designated as the “C zones,” one on each side of the M-line (Bennett et al., 1986).

1.2 Optical Microscopy

Optical microscopy was the primary tool for early studies of the structure and function of sarcomeres and continues to be an indispensable research tool for the field. Optical microscopy uses lenses to magnify light signals visible to one’s eye or a camera. There are two major categories of optical microscopy: transmitted light and fluorescence.

Transmitted light microscopy includes any mode where white light is used to illuminate a field of view. These modes are what most people think of in association with the word “microscope.” The light can be direct, as in brightfield microscopy, or it can be directed at an angle, as in differential interference contrast (DIC) or Nomarski microscopy (Allen & David, 1969). In all cases, the resulting image is comprised of light

that passes through the objects in the field of view (Figure 1.2-1A).

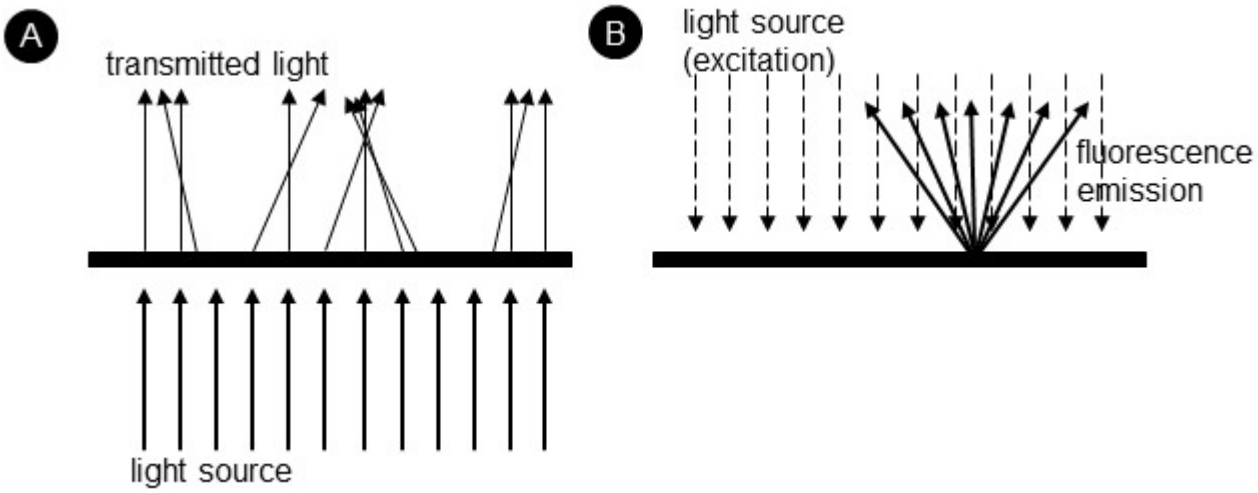

Figure 1.2-1. Transmitted Light and Fluorescence Microscopy

(A) Transmitted light microscopy relies on the detection of light which has passed through a sample. (B) Fluorescence microscopy relies on the detection of light emitted from a sample.

Contrast, which allows one to distinguish an object from the background noise, can be a challenge in transmitted light microscopy depending on the sample and the magnification. There are two main ways that optical contrast is generated: changes in light amplitude and changes in light phase (Zernike, 1935). At the micro-scale, most things have no discernable color and do not absorb much light (Goodwin, 2015). Changes in light amplitude are limited. Dyes or stains are commonly used to facilitate better contrast under transmitted light microscopy, such as the common histological stains hematoxylin and eosin or the bacterial Gram stain (Coico, 2006; Fischer et al., 2008). These introduce materials that absorb light a different amount than the background, creating a difference in light amplitude.

Where objects do not absorb any light and changes in light amplitude are small, light scattering within or around an object can create changes in phase significant enough to generate contrast. Transmitted light microscopy methods such as phase contrast intentionally increase these changes in phase to increase contrast (Zernike, 1935).

Fluorescence microscopy includes any mode that observes fluorescence, a phenomenon which occurs when energy from a specific wavelength of light activates a molecule to emit another, longer wavelength of light (Lichtman & Conchello, 2005). Fluorescence microscopy set ups must have a light source restricted to certain activating wavelengths and filters to restrict the wavelengths detected by eye or by a camera. The resulting image is not illuminated as in transmitted light microscopy but can be likened to seeing an airplane in the night sky: though it is dark and the airplane cannot be seen, the lights from the airplane are visible and traceable. Likewise, fluorescent microscopy observes the emitted light signals from fluorescent molecules called “fluorophores” (Figure 1.2-1B). Thus, a sample must contain some source of fluorescence for fluorescence microscopy to provide information.

Fluorophores can be native to a biological system or can be introduced. Native fluorophores contribute to autofluorescence, which may be considered the background signal. Introduced fluorophores can include fluorescent dyes such as DAPI, fluorescently-tagged probes such as antibodies or RNA probes, or fluorescent recombinant proteins such as GFP hybrids. In almost all cases where the fluorophore is non-native the researcher is aware of the molecule from which fluorescence is emitted, facilitating the localization and tracking of specific molecules of interest.

Transmitted light and fluorescence microscopies are often used in combination because they provide different kinds of information to the researcher. Transmitted light provides a broad picture, including the topography of the area of interest. So long as there is enough contrast, everything is visible (though everything may not be identifiable). Fluorescence, however, provides a picture of specific molecules of interest. The context remains dark, but the signal detected is traceable and originates from a known source. Thus, transmitted light microscopy is often useful for providing general context for information gathered from fluorescence microscopy.

1.3 Super-Resolution

All optical microscopy—both transmitted light and fluorescence—is limited in resolution to half the wavelength of light (Abbe, 1873). Light is diffracted as it passes around or through an object which introduces interference (Figure 1.3-1). Diffraction and interference prohibit the resolution of two points of light that reside within a certain distance from each other, called the “diffraction limit.”

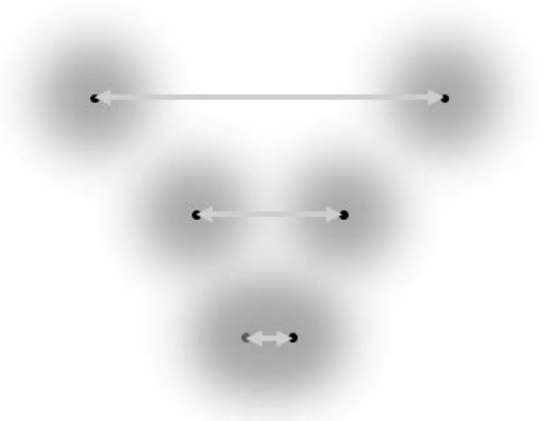

Figure 1.3-1. Diffraction Limit of Resolution

Resolution in light microscopy is limited by diffraction and interference of light passing around or emitted from objects.

Ernest Abbe mathematically described the diffraction limit (d) as the wavelength of light (λ) divided by double the numerical aperture (NA) of the optical path (Equation 1.3).

$$d = \frac{\lambda}{2\,NA}$$

Equation 1.3

NA is dependent on the refractive index of the medium between the lens and the sample, as well as the angle of light passing from the area of focus to the diameter of the lens, or the angular aperture (Figure 1.3-2). Both of these are factors that can be manipulated and thus optimized. Though air has a refractive index of 1.0, immersion media with higher refractive indices can increase NA. Likewise, changes in the design of a lens can increase NA. Wavelength, however, cannot be manipulated beyond a visible range and remain visible. Thus, optical microscopy set-ups employing visible wavelengths of light are fundamentally limited in resolution to 170-250 nm even if NA can be increased (Valli et al., 2021).

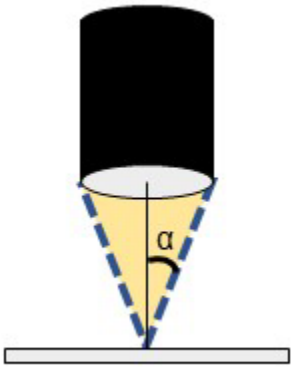

Figure 1.3-2. Angular Aperture Definition

Half the angular aperture is designated “α.”

Super-resolution microscopies are methods that circumvent the diffraction limit on optical microscopy, typically by using advanced methods of image acquisition and image processing. In ensemble super-resolution methods, the resolution of the entire image is improved (Valli et al., 2021). Stimulated emission depletion (STED), near field scanning optical microscopy (NSOM), and structured illumination microscopy (SIM) are ensemble methods that spatially manipulate the excitation of fluorophores to pinpoint their locations (Gustafsson, 2000; Wichmann & Hell, 1994). Single fluorophore super-resolution methods refine the locations of individual fluorophores, then reconstruct an image based on those refined locations. Single fluorophore methods include those such as dSTORM, PALM, and DNA-PAINT (Betzig et al., 2006; Heilemann et al., 2008; Jungmann et al., 2014). These require specific fluorophores which can be activated and deactivated either by a wavelength of light, reagent, or other condition. If only a small number of the fluorophores are activated at a given time, this allows the possibility that neighboring fluorophores are not activated simultaneously and can be resolved upon image reconstruction of the calculated centroids of each individual fluorophore.

1.4 Expansion Microscopy

Expansion microscopy (ExM) is a unique approach to super-resolution microscopy that manipulates the sample itself rather than the image acquisition process. In ExM, a biological sample is crosslinked and embedded into a swellable hydrogel. After the embedded sample undergoes a digestion step, water is added to the gel which causes it to expand (Figure 1.4-1). The expanding gel brings the crosslinked biomolecule fragments along with it, expanding the sample itself.

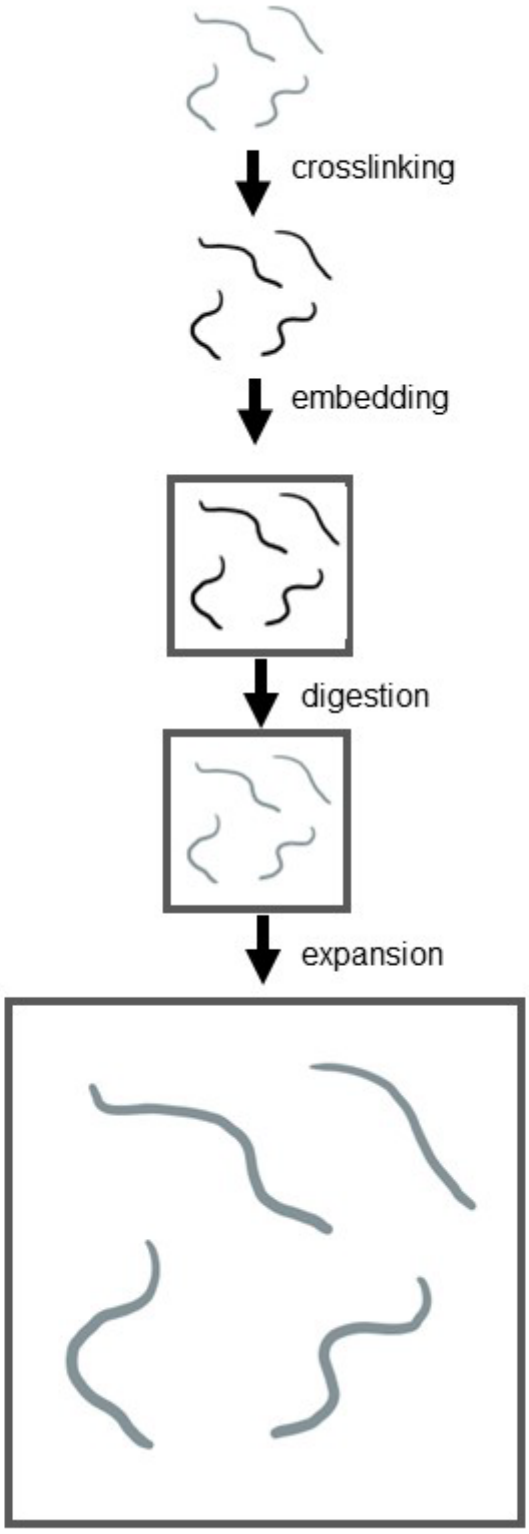

Figure 1.4-1. Expansion Microscopy Workflow

Expanded samples appear approximately four times their original size with a standard ExM preparation (Chen et al., 2015). The methods of image acquisition remain the same as in any typical optical microscopy, so the actual resolution and the NA of any particular set up are not improved. However, expansion results in a perceived increase in lateral resolution as fluorophores are physically separated from each other.

Since the original ExM publication in 2015 (Chen et al., 2015), several variations of ExM preparations have been developed. Protein-retention ExM crosslinks proteins directly to the hydrogel which facilitates antibody labeling (Tillberg et al., 2016). Iterative ExM involves reducing the original hydrogel for subsequent embedding an expansion within a secondary, or even tertiary hydrogel (Chang et al., 2017). Some have even attempted to image ExM preparations with other super-resolution imaging methods for maximum possible resolution (Gao et al., 2018; Shi et al., 2021; Zwettler et al., 2020).

ExM has proven to be helpful in imaging a wide range of biological sample types, from brain and liver slices to cell cultures to whole *Caenorhabditis elegans* (Sahabandu et al., 2019; Tillberg et al., 2016; Yu et al., 2020). ExM's accessibility is one reason it has seen such rapid development and application. This method does not require extensive and expensive imaging equipment, nor does it require very unique and specific fluorophores as other super-resolution methods do. A researcher can use common laboratory reagents to prepare a sample, then bring it to almost any fluorescence microscopy set-up for imaging. Sample preparation being responsible for attaining super-resolution sets ExM apart from every other super-resolution method.

1.5 Objective: Transmitted Light Super-Resolution

Due to the nature of the diffraction limit, it seems impossible to overcome it in transmitted light microscopy modes. It is not uncommon for transmitted light imaging to be done in tandem with super-resolution, but these partner images are not super-resolution images. While all other currently available super-resolution methods depend on properties of fluorescence to achieve super-resolution, ExM's super-resolution is independent of fluorophore properties. Because its approach involves manipulating the sample itself, ExM could be a feasible way of breaking the diffraction limit and bringing super-resolution to transmitted light microscopy.

The diversity of ExM variations have focused primarily on optimizing expansion factors and making up for deficits such as loss of fluorescence signal. There is no record of transmitted light imaging ever being combined with ExM, despite the pairing of transmitted light and fluorescence images being incredibly common in many types of localization studies. The aim of this thesis is to investigate ExM as a candidate for transmitted light super-resolution microscopy.

Transmitted light super-resolution microscopy could have virtually endless benefits and applications to biological research, especially in the fields of cell and molecular biology. Since fluorescence microscopies require labeling, current super-resolution methods will only ever reveal what can be labeled. Even when subcellular regions can be labeled by standard markers, the number of fluorescent color channels is limited (especially in single-fluorophore methods) limiting the information that can be gathered in a single set of images. Fluorescent markers used for context also depend on the markers to not interfere with the regular localization or labeling of the

biomolecule of interest, which is not always guaranteed. Gathering contextual information without using markers requires observing a biological sample's topography by transmitted light. ExM shows promise for facilitating transmitted light imaging with comparable resolution to fluorescent data.

Transmitted light super-resolution via ExM would also broaden the accessibility of ExM, and thus super-resolution also. Because ExM preparation only requires common biochemical reagents, ExM is already an accessible method. Institutions with no super-resolution facilities and little funding to rent them can still achieve super-resolution via ExM. Reducing the need for fluorescent microscopy set-ups would make ExM even more accessible.

The more accessible a technique, the easier it is for researchers worldwide to both improve the technique and gather new data with it. In the Root lab, the reported approach will aid in studying the localization of targeted peptides within the context of the myofibril and cardiac tissue at high resolutions. This has previously been impossible without employing markers for sarcomeric regions which may interfere with peptide binding. As it will do in the Root lab, transmitted light super-resolution will open the door to wide varieties of new possible data unattainable with current methods.

I hypothesize that preparing biological samples for protein-retention ExM will facilitate transmitted light imaging with increased detail useful for localizing fluorescent labels in the context of the sarcomere and other subcellular contexts. Here, rabbit myofibrils and mouse liver slices prepared for pro-ExM have been tested for their compatibility with transmitted light imaging. Increases in resolution have been described

in terms of the detail observed in each compared with unexpanded samples, and in expanded myofibrils, key sarcomeric features have been identified under brightfield.

CHAPTER 2

METHODS

2.1 Rabbit Myofibril Preparation

New Zealand white rabbits obtained from Charles River laboratories were euthanized under the supervision of a veterinarian according to protocols approved by the university's institutional animal care and use committee. In a cold room, fresh muscle tissue was harvested from the rabbit and passed through a meat grinder and submerged in borate buffer (0.08 M, pH 7.1). The mixture was diluted with more borate buffer to reach a concentration of approximately 10g/L. A cold blender was used to homogenize the mixture for 20 seconds.

The homogenized mixture was washed with borate buffer three times by centrifuging at 1500xg, decanting the supernatant, and resuspending in fresh borate buffer. All centrifugations occurred at 0°C for one minute. Large contaminants were removed from the resulting pellet by centrifuging at 400xg. The supernatant, containing the myofibrils, was centrifuged at 1500xg to capture the myofibrils in the pellet. This pellet was resuspended in 100 mL of borate buffer before the last centrifugation at 400xg. The final pellet was discarded, and the final supernatant containing the myofibrils was stored at -20°C in 50% glycerol.

2.2 Antibody and Peptide Incubation

To identify sarcomeric structures, rabbit myofibrils were labeled prior to expansion at 4°C overnight with 10.4 μM (MF30) or 75 μM (CH1) fluorescently-tagged antibody in phosphate-buffered saline (PBS) at pH 7.2. MF30 and CH1 obtained from

the Developmental Studies Hybridoma Bank (DSHB) were used to label myosin and tropomyosin, repsectively. MF30 was deposited to the DSHB by Fischman, D.A. (DSHB Hybridoma Product MF30). CH1 was deposited to the DSHB by Lin, J.J.-C. (DSHB Hybridoma Product CH1). Myofibrils were washed with PBS twice for 2 minutes each before continuing for pro-ExM preparation.

Antibodies were conjugated to their respective fluorophores by reacting with 10 mg/mL tetramethylrhodamine isothiocyanate (TRITC) in N-N-dimethylformamide at room temperature for one hour. Unreacted TRITC was removed via Micro Bio-Spin chromatography column (BioRad, Hercules, CA) into PBS according to package instructions. Concentrations of the resulting antibodies and their conjugation efficiency were calculated from their absorbance at 280 nm for antibodies (extinction coefficient = 170,000 M-1 cm-1), 551 for TRITC (extinction coefficient = 100,000 M-1 cm-1).

A synthetic peptide designed to bind specifically to tropomyosin was commercially synthesized by Biosynthesis (Lewisville, TX) with a fluorescent 5-carboxytetramethylrhodamine (TAMRA) tag on the N-terminus. To localize this peptide within the sarcomere, 3 µg of solid peptide was suspended in 1 mL PBS and incubated with rabbit myofibrils overnight at 4°C. These were washed with PBS and prepared for pro-ExM.

2.3 Pro-ExM with Rabbit Myofibrils

Rabbit myofibrils were incubated with 0.1% glutaraldehyde (Sigma-Aldrich, St. Louis, MO) in PBS for one hour at room temperature, then washed with PBS. Then these were incubated in monomer solution (86 mg/mL sodium acrylate (Sigma-Aldrich),

25 mg/mL acrylamide (Fluka BioChemika, Buchs, Switzerland), 1.5 mg/mL N,N'-Methylenebisacrylamide (Sigma-Aldrich), 0.117 g/mL NaCl (EM Science, Gibbstown, NJ), 1x PBS) for 20-30 minutes on ice. To facilitate embedding the monomer-linked myofibrils, a 1-1.5 cm by 1-1.5 cm gel chamber was constructed from glass coverslips. After myofibrils were transferred to the chamber, the chamber was filled with a mixture of 100 µL monomer solution, 2 µL 0.5% TEMPO (Sigma-Aldrich), 2 µL 10% TEMED (Sigma-Aldrich), and 2 µL 10% ammonium persulfate (Sigma-Aldrich). The gel chamber was quickly sealed with another coverslip and left to polymerize for at least one hour at room temperature.

Polymerized gels were treated with proteinase K (New England BioLabs, Ipswich, MA) diluted 1:2500 in digestion buffer (50 mM Tris (Research Organics, Cleveland, OH), 1 mM EDTA (Sigma-Aldrich), 4 M urea (Research Organics), 2 mM $CaCl_2$ (MCB Reagents, Gibbstown, NJ), 0.8M guanidine HCl (Spectrum Quality Products, Gardena, CA), 0.5% Triton X-100 (Research Organics)) overnight at 37-40°C. Successive 20-minute washes with Millipore water in a large dish removed digestion buffer and expanded the gels. Washes were repeated until gels reached their maximum dimensions, then expanded gels were sandwiched between two poly-lysine-coated glass coverslips for image acquisition.

2.4 Pro-ExM with Mouse Liver

Flash-frozen livers from mice treated with anti-myosin peptides were acquired from collaborators (Dr. Kenneth Campbell's lab at University of Kentucky). Mouse liver was embedded into O.C.T. Compound (Scigen Scientific, Gardena, CA) and sectioned

into 100 μm slices using a cryotome (Leica CM1950). Slices were transferred to glass coverslips for handling. These slices underwent pro-ExM preparation as in “pro-ExM,” except that glutaraldehyde crosslinking and monomer incubation steps were extended overnight to allow thorough diffusion of these reagents through the tissue.

2.5 Pro-ExM with Alkaline Phosphatase Labeling

Samples of rabbit myofibrils prepared for alkaline phosphatase (AP) labeling were incubated in MF30 as described in “Antibody Labeling.” After only primary incubation, these samples underwent glutaraldehyde crosslinking, embedding, and digestion as in “Pro-ExM.” Following digestion, the sample was washed with PBS three times for 5 minutes each with gentle shaking. The washed gel was incubated with 1.7-13.3 μg/mL AP-conjugated anti-mouse secondary antibody (Sigma-Aldrich A3562) at room temperature, gently shaking overnight. The sample was washed again with PBS three times for 5 minutes each before expansion as in “Pro-ExM.” The expanded sample was submerged in SigmaFAST staining solution prepared by package instructions (Sigma-Aldrich) until blue-purple color was visible by eye. The stained, expanded samples were sandwiched between two poly-lysine-coated glass coverslips for image acquisition.

For comparison to expanded myofibrils, control myofibrils labeled with MF30 primary antibody skipped pro-ExM preparation and were prepared for AP-labeling as described above. These were wet-mounted to a standard glass slide for imaging.

2.6 Image Acquisition

A Zeiss Axiovert 200M (Oberkochen, Germany) was used to acquire images of expanded gels to allow for increased working distance. Images were captured through a PlanApo 20x objective lens (numerical aperture = 0.8) or a C-Apo 40x water-immersion objective lens (numerical aperture = 1.2) in combination with a 1.6x tube lens. Low magnification images were captured through a 5x objective lens in combination with a 1.0x tube lens. A Hamamatsu C 9100-02 EMCCD digital camera (Hamamatsu Photonics K.K., Hamamatsu, Japan) was used to capture black and white images including brightfield, confocal, and epifluorescence channels. For confocal imaging, TRITC and TAMRA fluorophores were imaged using a 532 nm solid state laser and a 585 +/- 40 nm emission filter. Color images were captured as red, blue, and green channels with a SPOT RT SE6 Monochrome camera (Diagnostic Instruments Inc., Sterling Heights, MI) with a VariSpec liquid crystal tunable filter (Cambridge Research & Instrumentation, Inc., Hopkinton, MA).

A Zeiss Axioscope 5 equipped with a 40x A-Plan air immersion objective lens was used for polarized light microscopy. The polarizer and analyzer were positioned perpendicular to each other so that the polarized incident light could not reach the camera. Images were captured of each specimen as it was rotated in 45-degree increments over a total 180 degrees, both with and without a wave plate in place, using a Zeiss Axiocam 208 color camera.

2.7 Image Processing

Each image shown was adjusted for contrast and brightness in ImageJ (Schindelin et al., 2012) to optimize visualization of features. These adjustments were applied to duplicate files only so that original pixel values were preserved for quantitative analysis. To localize fluorescent labels in the context of transmitted light structures, brightfield and confocal channels of the same field of view were combined and compared.

To create sarcomere averages, 30 – 100 selections including both brightfield and confocal channels from a single image were concatenated and then averaged into one image (Figure 2.7-1). To create half-sarcomere averages (60-200 selections), the resulting average sarcomere was flipped horizontally and averaged with the original.

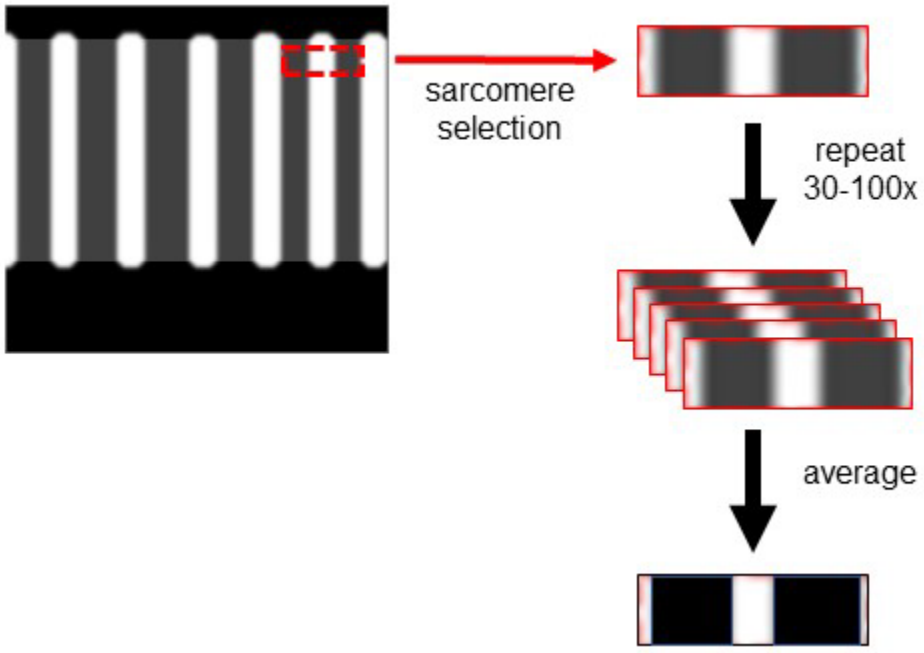

Figure 2.7-1. Sarcomere Averaging Workflow

Pixel grey values were plotted against the x-coordinate (μm) to quantify average sarcomeric patterns. In brightfield images, grey value describes relative transmittance while in confocal images it describes relative fluorescence intensity.

2.8 Quantifying Expansion Factor

Image scales were set according to the known pixels/μm ratio of the lenses used. To take expansion heterogeneity into account, for each image, the average of 3-5 A band width measurements was divided by 1.5 μm, the width of an unexpanded A-band (A. F. Huxley & Niedergerke, 1954). This ratio of expanded/unexpanded values were called "expansion factor." Thus, a sample with an expansion factor of 4x would have an A band appearing 6 μm wide.

2.9 Quantifying Contrast in Brightfield Images

Images were chosen for contrast quantification which contained clear myofibril striations, a clearly visible background. These images were each captured with the ideal illumination for that field of view but used the same optical path and camera settings. A bias frame was also captured with the same camera settings but without illumination or anything in the optical path. For each image, an area including the myofibril and excluding the background was selected and pixel grey values within the selected area were plotted using ImageJ as a histogram. After subtracting the bias frame mean from each pixel grey value, contrast ratios for each image were calculated by dividing the maximum grey value by the minimum grey value. The range of grey values from the whole image was used to quantify contrast for transmitted light images.

A two-tailed t-test assuming unequal variances was performed to compare the contrast, in terms of pixel grey value range, between images of expanded myofibrils and of myofibrils that did not undergo any preparation for expansion. A p value less than 0.05 was considered to indicate a significant difference.

The relationship of contrast to expansion factor was determined by plotting contrast ratio against expansion factor. Regression analysis was run in Microsoft Excel to determine the correlation coefficient (r) and describe the significance of the correlation with an ANOVA. A p value less than 0.05 was considered to indicate significance.

2.10 Determining Anisotropy from Polarized Light Microscopy Images

Anisotropic materials allow different amounts of light to pass through a polarized light microscope depending on the angle that material is rotated. The average pixel grey values in an area of interest were compared between images of the same sample at rotation angles corresponding to the maximum and minimum amount of light allowed to pass through, which are 45° relative to each other. The difference in these values was expressed in terms of percent difference. Average percent difference was compared between myofibrils prepared and not prepared for pro-ExM to determine the relative amount of anisotropy retained after expansion.

2.11 Predicting Sarcomeric Ultrastructure

Ratios of I/A band widths at various sarcomere lengths (SL) were estimated by the assumption that SL=A+I, and that the A band retains a consistent length of 1.5 μm

(A. F. Huxley & Niedergerke, 1954). The relationship between I/A and SL was plotted and fitted to a linear equation, which was called the standard.

To determine which striations observed in expanded sarcomeres corresponded to the A and I bands, 5-12 measurements of each striation type (appearing wider or thinner) and each sarcomere length were taken per image. SL was normalized according to the expansion factor for that image. Average widths were used to plot ratios of these band widths against sarcomere length. Two plots were created: one assuming the wider striation observed was the A band, and one assuming this striation was the I band. The plot with an equation similar to the one found from the standard revealed which striations matched the A and I bands.

CHAPTER 3

RESULTS

3.1 Transmitted Light Properties are Preserved in Expansion Microscopy

For a biological sample to expand in hydrogel, its pieces must be cleaved to allow for separation. In an ExM preparation this is accomplished by protease digestion, and it can be assumed that digesting the sample will destroy the intrinsic optical properties which allow it to be seen with transmitted light. This work has found that the forementioned assumption is false: expanded samples including myofibrils and liver tissue slices are detectable with in brightfield and DIC microscopy.

Compared to unexpanded myofibrils, expanding myofibrils revealed more sarcomeric structural features and increased detail within features. In unexpanded myofibrils, the A and I bands are seen as alternating dark and light striations (Figure 3.1-1A, 3.1-2A). In expanded myofibrils, A bands clearly appeared wider, and Z-discs became apparent (Figure 3.1-1B, 3.1-2B). Averaging expanded sarcomeres revealed an A band more reminiscent of a plateau with a dip near the center than the hills that are seen in unexpanded sarcomeres (Figure 3.1-2).

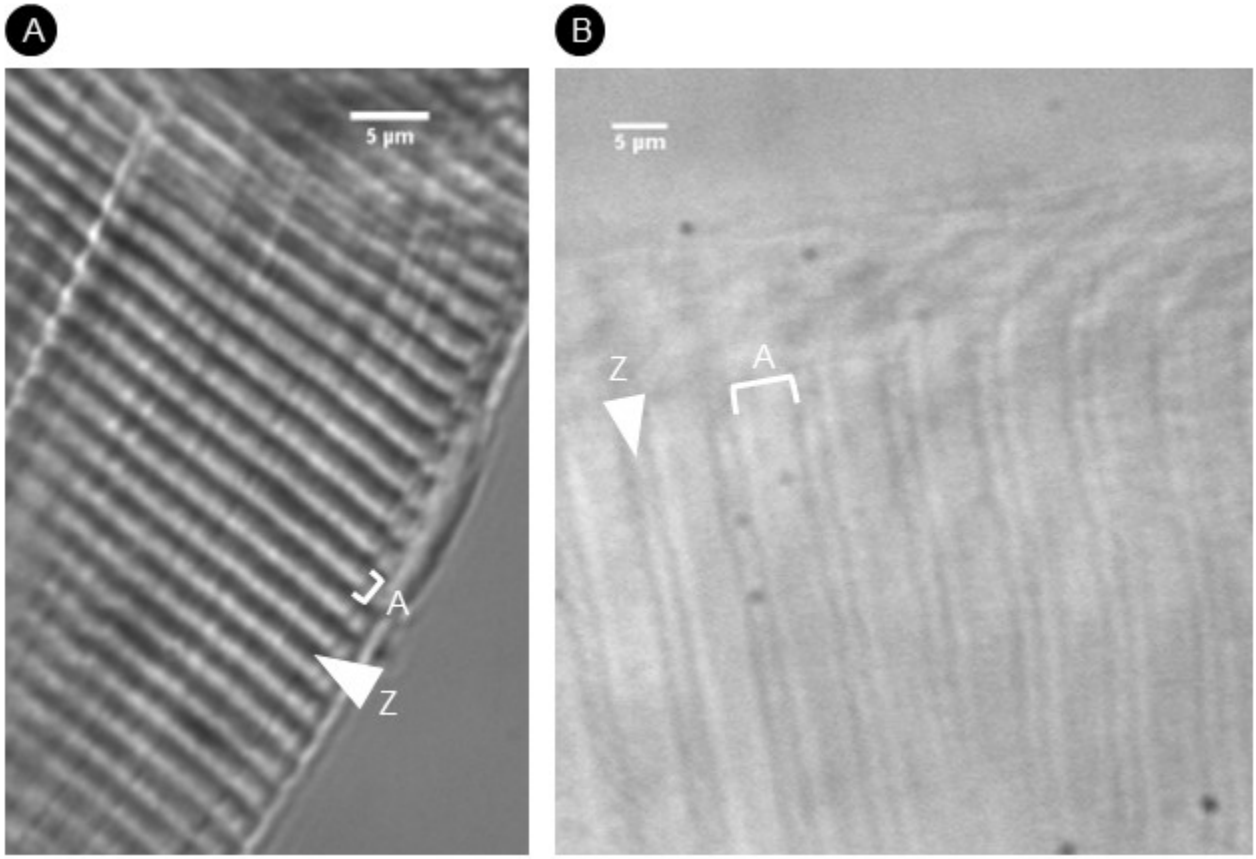

Figure 3.1-1. Expansion of Myofibrils under Brightfield Microscopy

Representative brightfield images of myofibrillar bundles unexpanded (A) and expanded 3.4x (B). All are adjusted for brightness and contrast to reveal optimal detail. Brackets indicate the A band, and arrowheads indicate the location of the Z-disc, at the center of the I band. Scale is actual, not adjusted for expansion.

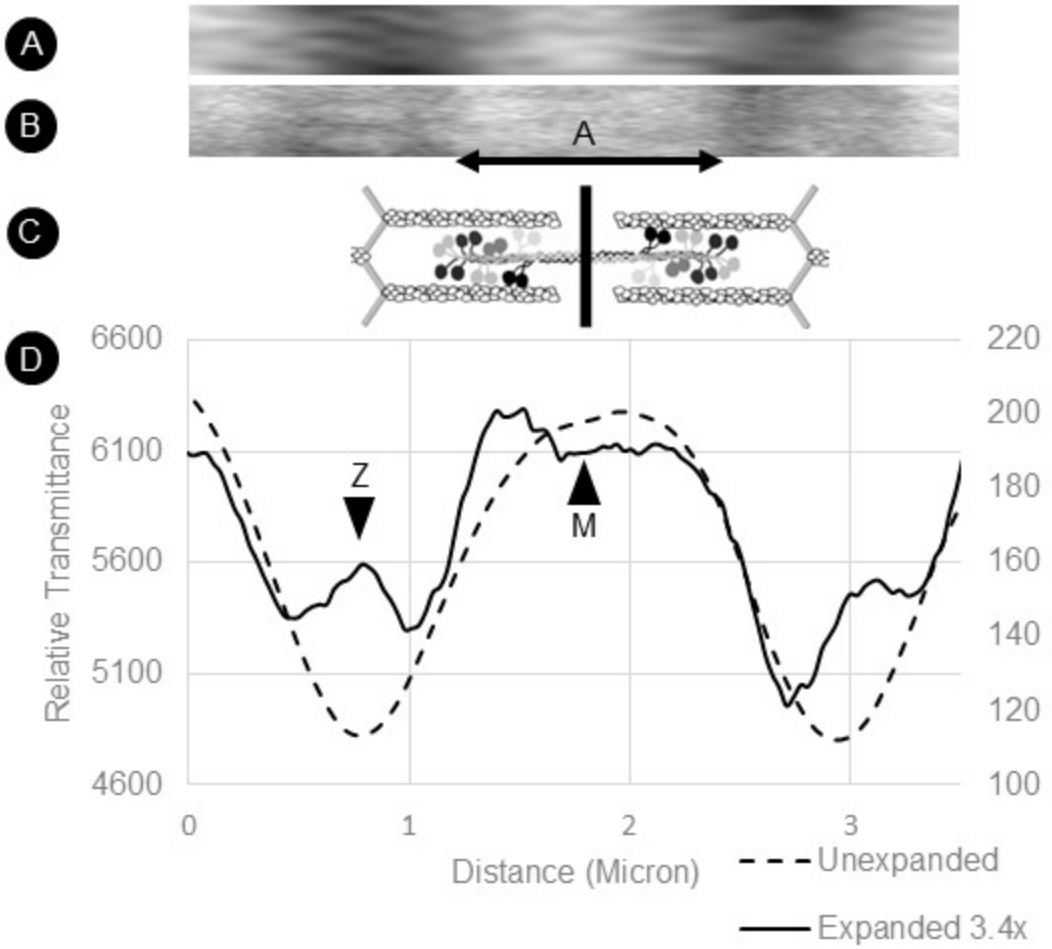

Figure 3.1-2. Expansion of Sarcomeres under Brightfield Microscopy

Selections of a single sarcomere from an unexpanded myofibril (A) and from a myofibril expanded 3.4x (B), centered on the M-line and aligned with sarcomere diagram (C). (D) Profiles of selections (A-B) aligned with the M-line in the center. Distances shown for selection (B) are adjusted according to expansion factor.

To determine whether other biological samples would be observable under transmitted light after expansion, mouse liver tissue slices were also prepared for pro-ExM. Nuclei were visible under brightfield microscopy (Figure 3.1-4). While nuclei in unexpanded liver slices averaged about 4.5 μm in diameter, nuclei in expanded liver

slices averaged 17.6 µm and indicated a 3.9x expansion. Some cell interfaces were also visible after expansion (Figure 3.1-4). These revealed cell shapes consistent with hepatocytes.

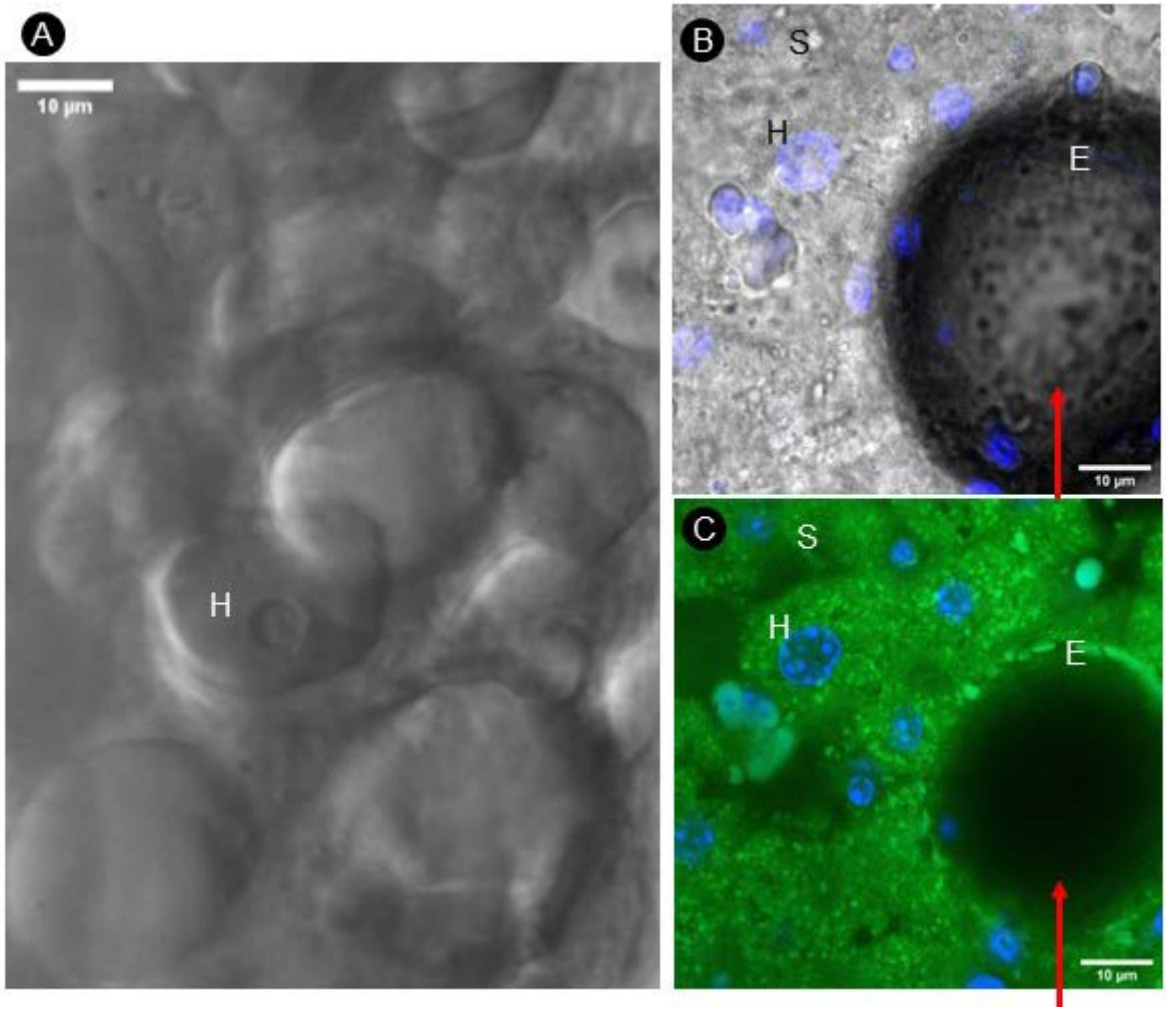

Figure *3.1-3*. Liver Slices under Brightfield Microscopy

(A-C) Representative images of mouse liver slices before expansion. Red arrows indicate blood vessels. H indicates hepatocytes, E indicates endothelial cells, and S indicates stellate cells containing fat vacuoles. (A) Brightfield. (B) Brightfield and DAPI staining. (C) Green fluorescence from FITC-conjugated peptide and DAPI staining.

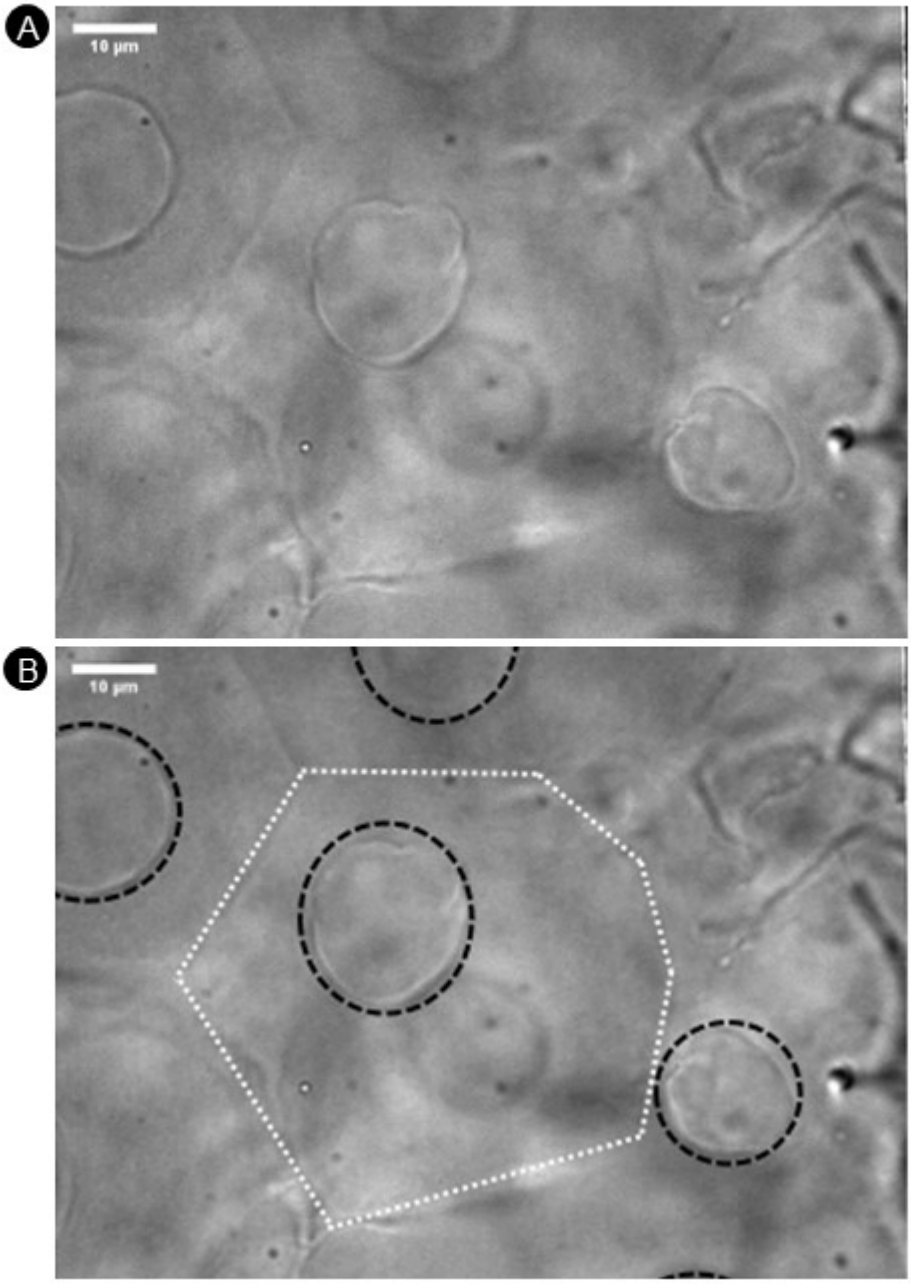

Figure 3.1-4. Expansion of Liver Slices under Brightfield Microscopy

(A-B) Representative image of mouse liver slices expanded ~3.9x. Scale is actual, not adjusted for expansion. (B) Nuclei are indicated by black dotted lines, and cell interfaces indicated by white dotted lines. Each image is adjusted for brightness and contrast to reveal optimal detail.

3.2 Optical Contrast is Decreased in Expansion Microscopy

Though expanded myofibrils consistently showed more detail than unexpanded myofibrils, they also consistently showed decreased optical contrast when compared qualitatively (Figure 3.2-1). There is also a significant quantitative difference ($p = 0.006$) between the contrast ratio of images of expanded myofibrils and images of myofibrils that have not undergone expansion preparation (Figure 3.2-2A).

Because the difference in contrast is apparent between myofibrils prepared for expansion and those not prepared, it was hypothesized that contrast may decrease with increasing levels of expansion. When comparing images of myofibrils with various expansion factors, contrast ratio was found to have a significant, though only moderate, positive correlation ($r = 0.54$, $p = 0.001$) to expansion factor (Figure 3.2-2B). However, when comparing only images of expanded myofibrils, no significant correlation ($r = 0.28$, $p = 0.18$) was found between contrast ratio and expansion factor. Therefore, while the process of pro-ExM has an influence on the contrast observed in brightfield microscopy, the expansion factor does not. This implies that decreases in contrast may be attributed to digestion more so than to expansion itself.

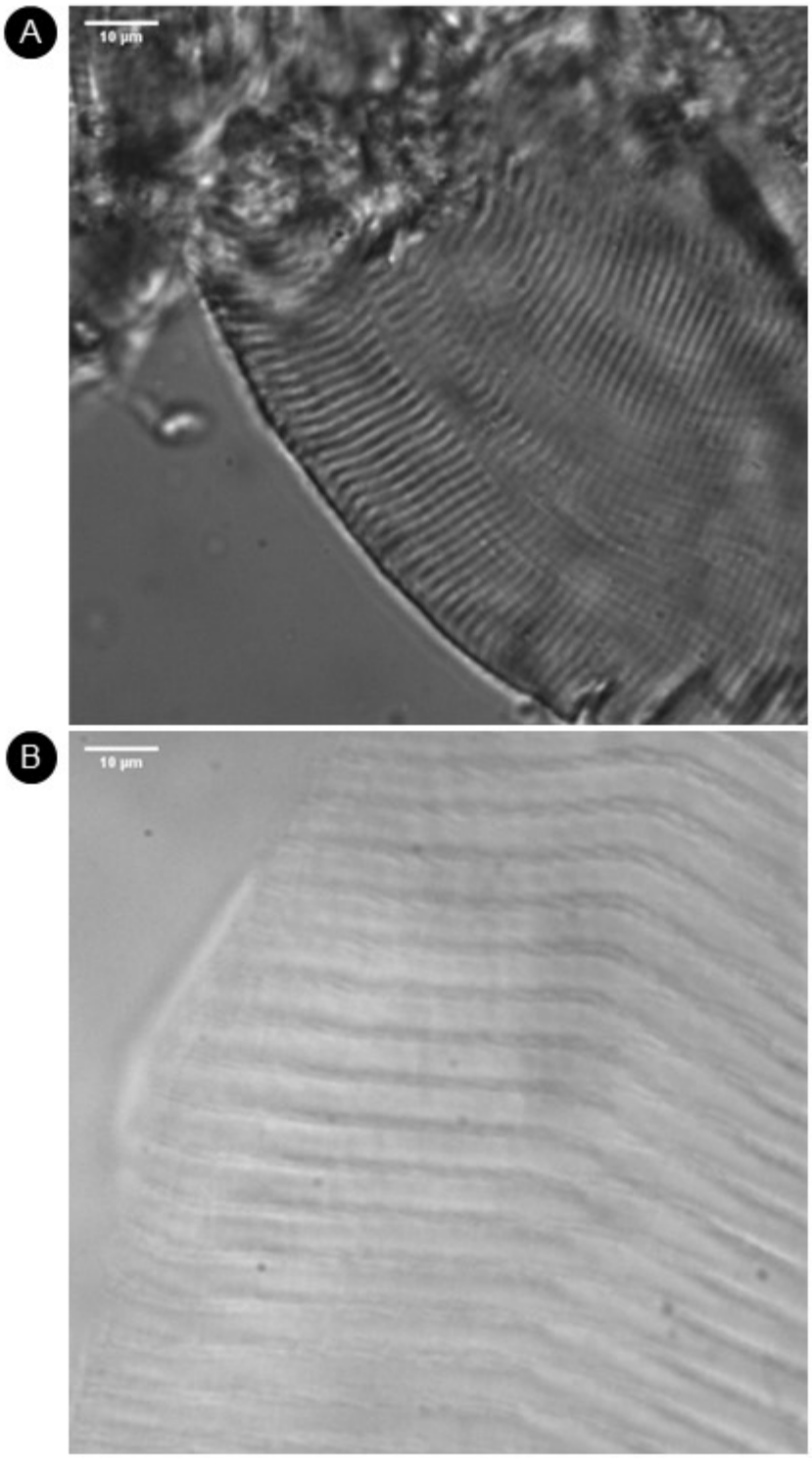

Figure 3.2-1. Contrast Decreases with Expansion Microscopy

(A-B) Unprocessed brightfield images representative of unexpanded myofibrils (A) and expanded myofibrils (B, expanded 2.03x). Scale is actual, not adjusted for expansion.

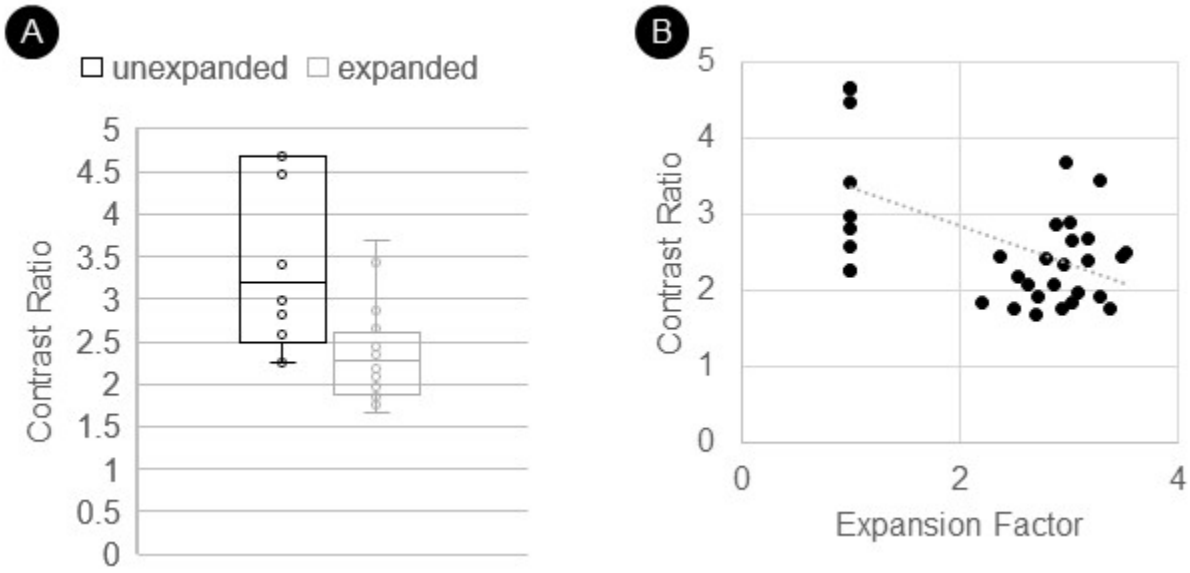

Figure 3.2-2. Relationship Between Contrast and Expansion

(A) Contrast ratio in images of unexpanded myofibrils and expanded ones. (B) Contrast ratio in images of myofibrils is moderately correlated to expansion factor.

3.3 Using Chromogenic Enzymes for Labeling in Expansion Microscopy

Stains are commonly used to increase contrast using brightfield microscopy modes. Most are nonspecific, but specific labeling of proteins is commonly done by immunohistochemistry, which employs antibodies conjugated to chromogenic enzymes such as horse radish peroxidase or alkaline phosphatase to localize a stain. Antibody labeling with an alkaline phosphatase system was combined with expansion microscopy in hopes of increasing the contrast of brightfield images and facilitating brightfield-accessible labeling.

To avoid washing away the resulting stain during the expansion process, the alkaline phosphatase substrate solution was added after expansion. However, the

substrate solution reversed expansion such that expansion factors were only able to reach approximately 2x, half of what is typical for pro-ExM.

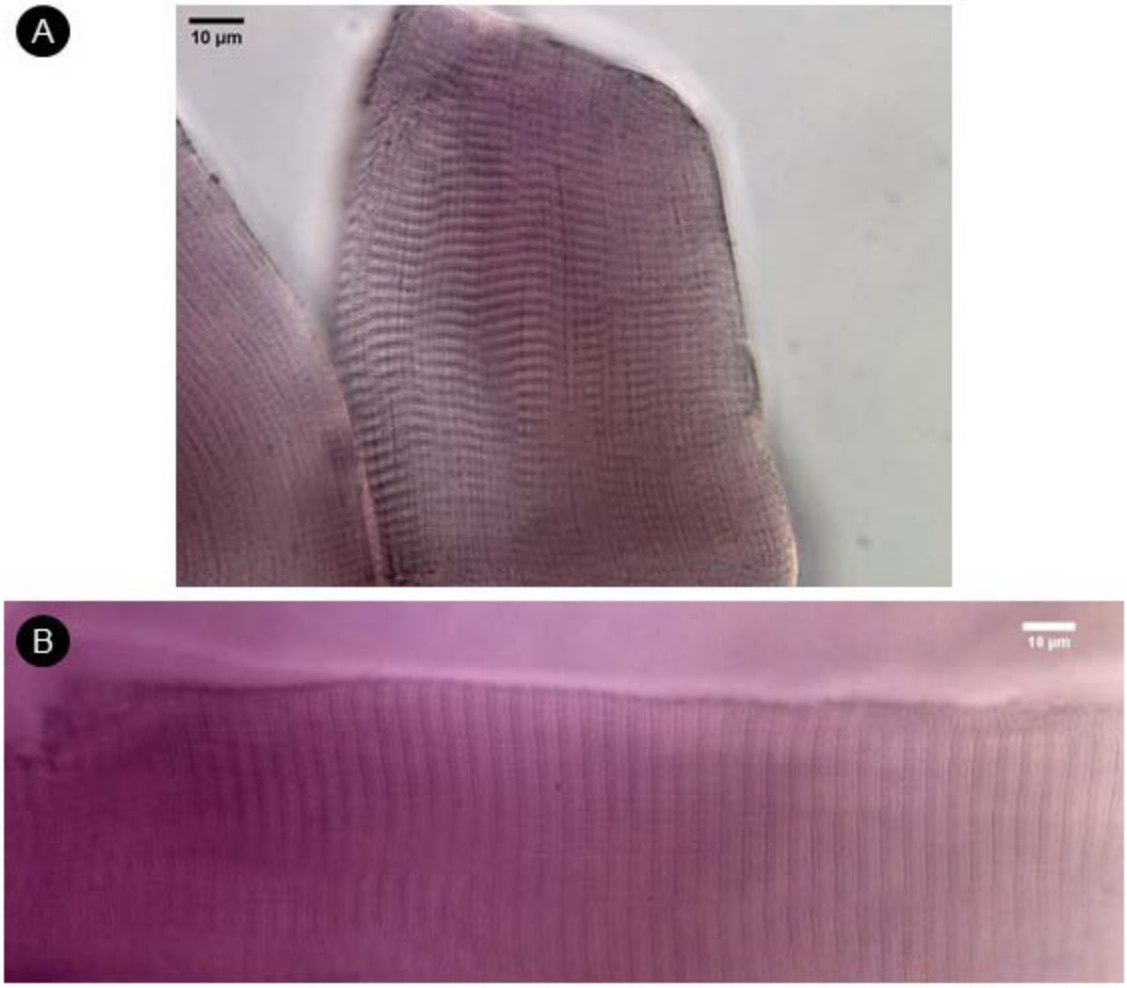

Figure 3.3-1. Immunohistochemical Staining with Expansion Microscopy Representative RGB images of myofibrillar bundles labeled using MF30 and a secondary antibody conjugated with alkaline phosphatase. (A) Control, unexpanded myofibrillar bundle. Staining is exclusive to the myofibril and does not infiltrate the background. (B) Expanded myofibrillar bundle. Staining is dramatically uneven within a single myofibrillar bundle and permeates the background.

While immunohistochemical stains facilitated easier visibility in expansion microscopy compared to no staining, it also resulted in non-specific labeling and was thus unreliable for determining the location of specific proteins (Figure 3.3-1).

3.4 A Band Anisotropy is Not Retained through Expansion

To determine whether protein is preserved through the pro-ExM preparation process, A band anisotropy was detected in expanded myofibrils using polarized light microscopy. The A bands of a sarcomere are known to be anisotropic, while the I bands are isotropic (A. F. Huxley & Niedergerke, 1954).

Control myofibrils were confirmed to display anisotropy at the A bands (Figure 3.4-1), with an average 87.5% difference between the minimum and maximum amount of light allowed to pass through the A bands at different angles of rotation relative to the light source.

However, no significant anisotropy was detected at the A bands in expanded myofibrils (Figure 3.4-2). There was an average 6.5% difference between the minimum and maximum amount of light allowed to pass through the A bands at different angles of rotation relative to the light source. This difference is 13x smaller than the difference seen in control myofibrils and is within a range that can be attributable to random variation. Thus, expanded A bands were determined to be isotropic. Empty hydrogel is also isotropic, with only an average 0.08% difference between the minimum and maximum amount of light allowed to pass through the A bands at different angles of rotation relative to the light source (Figure 3.4-3).

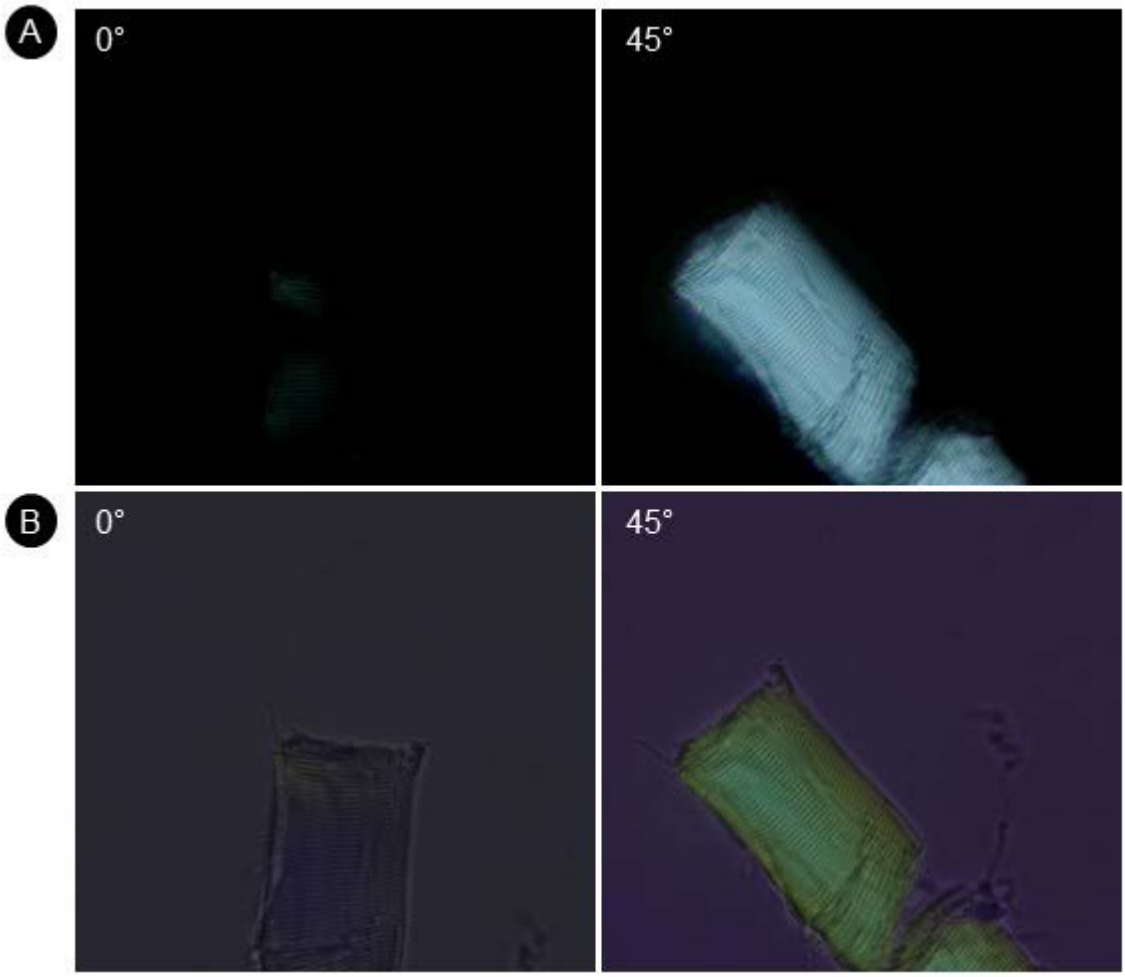

Figure 3.4-1. Polarized Light Microscopy of Control Myofibrils

Control myofibrils imaged under polarized light microscopy. Images in row A were taken using no extra filter or adjustments, and images in row B were taken using a wave plate. Each image is 1588 μm x 1588 μm.

Lack of anisotropy in expanded A bands suggests that not enough protein is retained through pro-ExM preparation to generate sufficient optical contrast in transmitted light microscopy modes. Contrast may instead be generated by the shape of the hydrogel itself, which has formed around the sample.

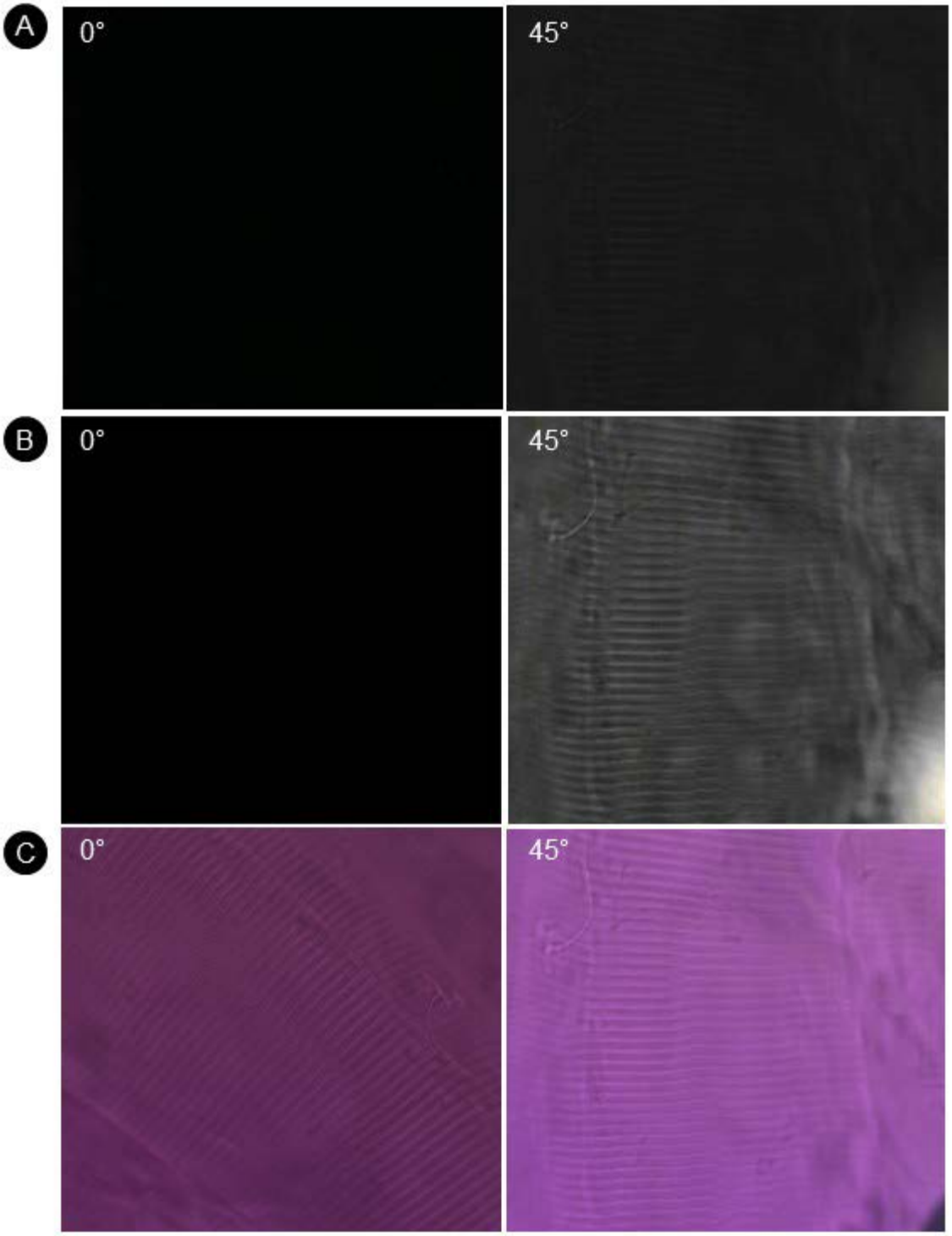

Figure 3.4-2. Polarized Light Microscopy of Expanded Myofibrils

Expanded myofibrils imaged under polarized light microscopy. Images in row A were taken using no extra filter or adjustments. Images in row B are the same fields of view with increased contrast applied digitally, and images in row C were taken using a wave

plate for additional contrast. A bands demonstrate no anisotropy. Each image is 1588 µm x 1588 µm. Expansion factor = 2.8x.

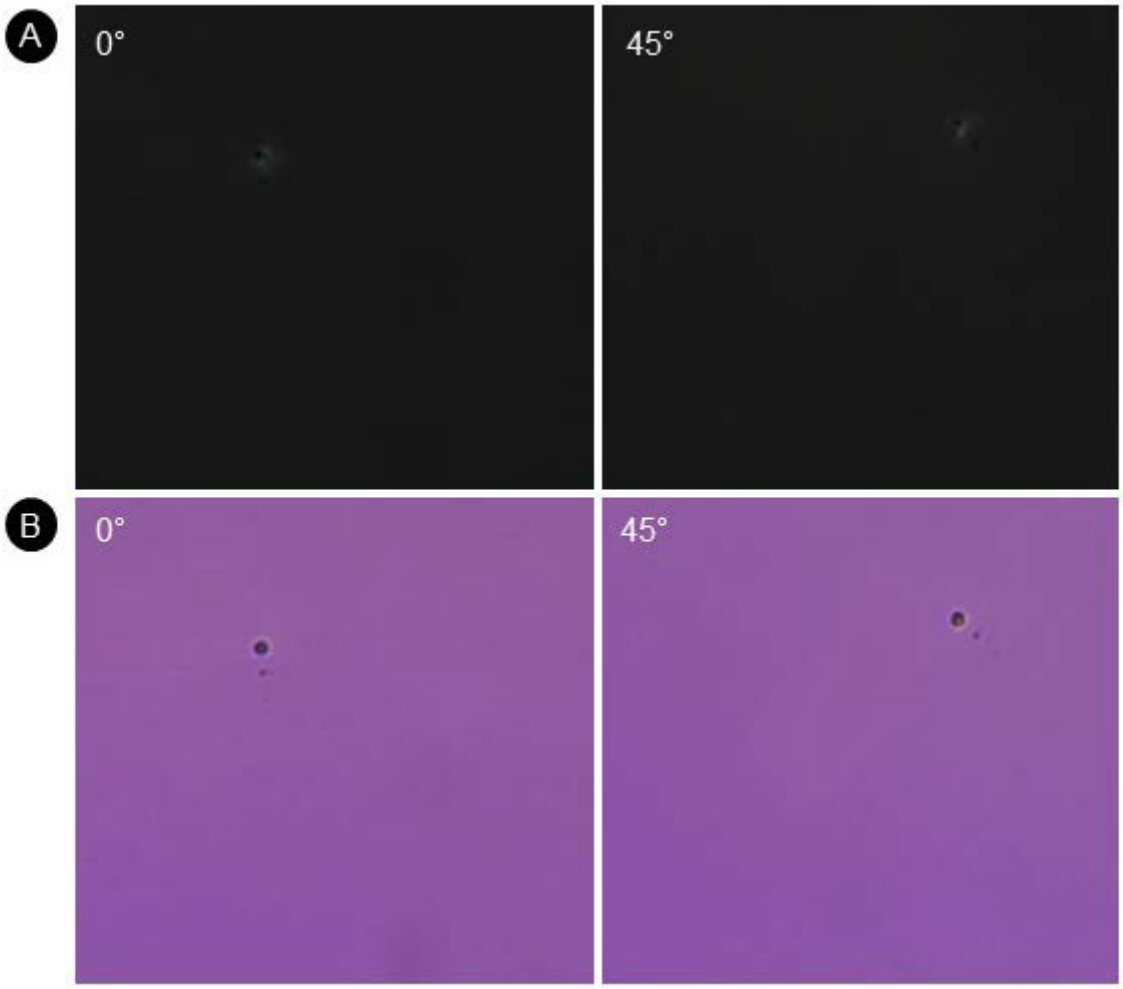

Figure 3.4-3. Polarized Light Microscopy of Acrylamide Hydrogel

Empty hydrogel imaged under polarized light microscopy. Images in row A were taken using no extra filter. Images in row B are the same fields of view, taken using a wave plate for additional contrast. Hydrogel demonstrates no anisotropy. Each image is 1588 µm x 1588 µm.

3.5 Predicting Sarcomeric Features in Transmitted Light After Expansion

Though expanded myofibrils at lower magnifications appear much like unexpanded ones at higher magnifications, it cannot be assumed that all sarcomeric features appear the same post-expansion. Differences in the extent of digestion and changes in microenvironment from hydrogel embedding and expansion could potentially alter the appearance of features. To investigate the post-expansion appearance of known sarcomeric features under brightfield microscopy, two complementary approaches were used: striation measurements and immunolabeling.

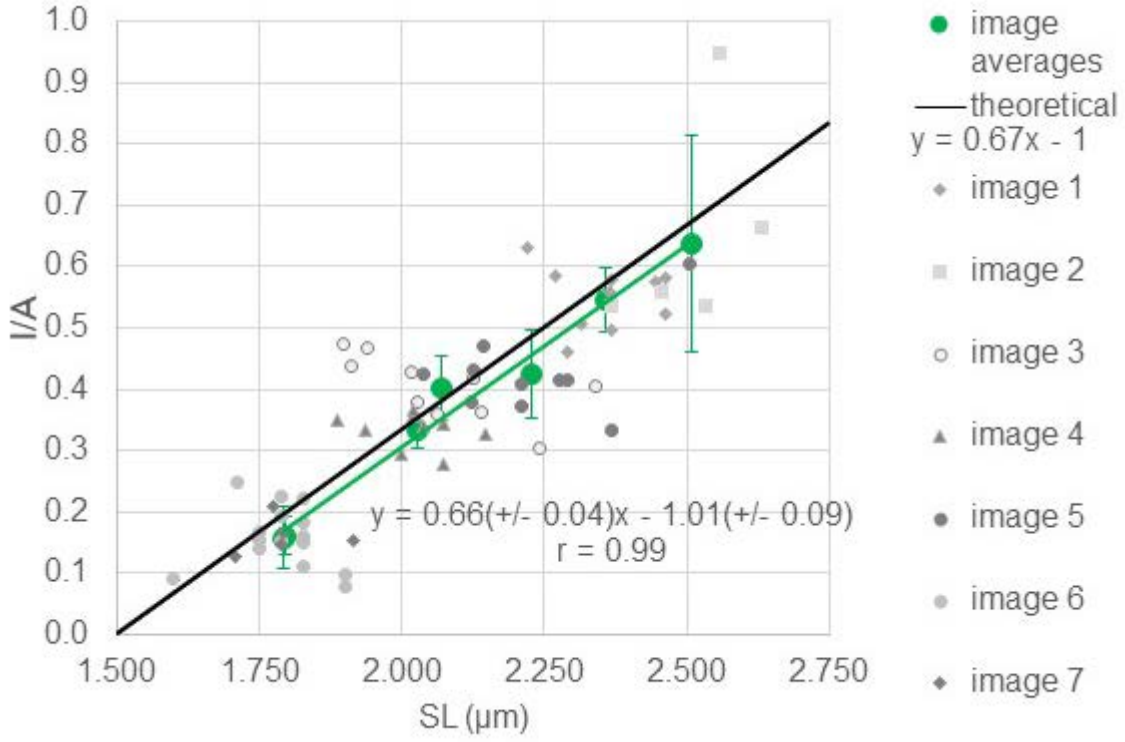

Figure 3.5-1. Sarcomere Length and I/A band Ratio in Expanded Myofibrils

Sarcomere length (SL) is linearly related to the theoretical ratio of I band width to A band width (I/A), as shown in black. SL is linearly related to the ratio of expanded thin band width to thick band width by the same equation, shown in green, when the thin band observed in brightfield is assumed to be the I band, and the thick band the A band.

The width of the A band remains constant at all sarcomere lengths, but the width of the I band changes as the sarcomere contracts and relaxes (A. F. Huxley & Niedergerke, 1954). Thus, the ratio of I/A band changes with sarcomere length in a predictable manner (Figure 3.5-1, black line). Expanded sarcomeres clearly show a wider band and a thinner band, though each of these can appear lighter or darker than the other depending on their illumination. It was determined that the I band was the thinner band and the A band was the wider band, since plotting the ratio of their widths against sarcomere length yielded an equation similar to the theoretical standard (Figure 3.5-1, green line). When it was assumed that the I band was the thicker band, the resulting plot shared almost nothing in common with the theoretical standard.

The range of sarcomere lengths resulting from correct identification of the A band, once adjusted for expansion factor, was physiologically reasonable (1.77 – 3.02 μm). The range resulting from opposite identification was unreasonable, yielding sarcomere lengths up to 5 μm, confirming that the expanded A band does appear wider than the I band under brightfield microscopy.

A similar approach was repeated to identify the hypothesized overlap region and H zone, other features that change predictably with sarcomere length. However, no trends were observed from these measurements.

3.6 Characterizing Sarcomeric Features in Transmitted Light After Expansion via Fluorescent Antibody Labeling

To confirm predictions based on theoretical sarcomere measurements, myosin and tropomyosin in rabbit myofibrils were labeled using fluorescent antibodies and prepared for pro-ExM. Though autofluorescence in myofibrils is amplified at the A band

(Figure 3.6-1), antibody labeling against myosin demonstrated a more intense fluorescent signal than autofluorescence and was certainly more detailed. Labeling with this antibody resulted in a peak in signal at the M-line, the center of the A band, and a dip in signal consistent with competition for binding in the C-zone (Figure 3.6-3). Both of these features have been observed and characterized by others (Quedan & Root, 2022). Myosin antibody labeling agreed with the prediction that the plateau-like, wide band observed under brightfield microscopy is the A band or thick filament (Figures 3.6-2 and 3.6-3).

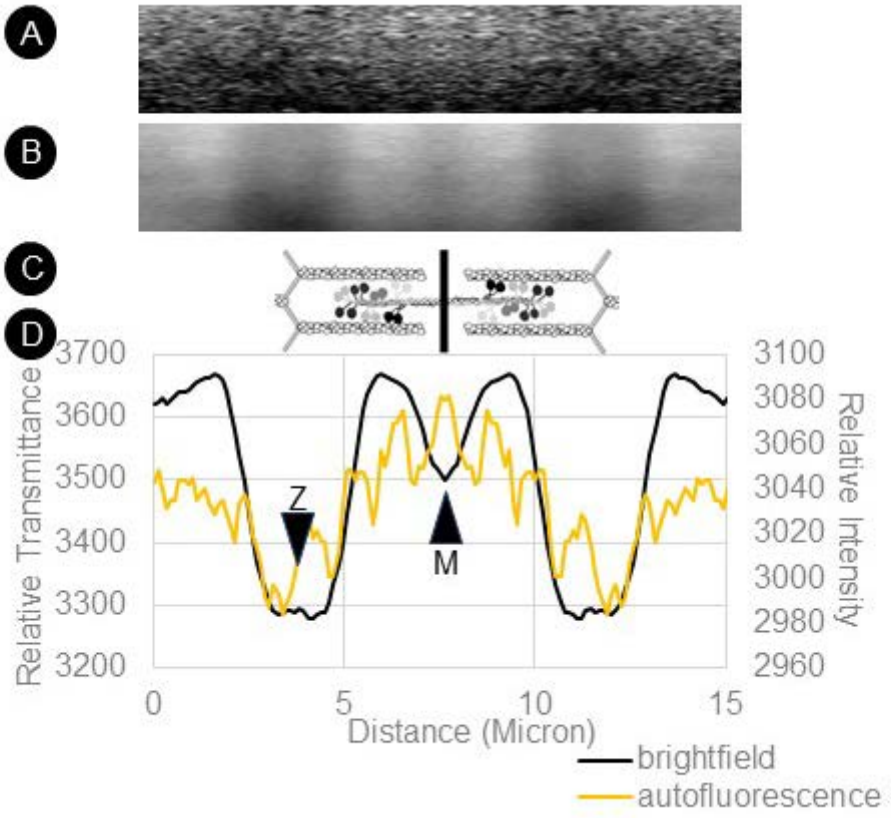

Figure 3.6-1. Autofluorescence Profile of the Expanded Sarcomere

(A) Autofluorescence signal of a sarcomere expanded ~3.3x upon excitation with a 532 nm laser through a 580 nm emission filter. (B) Single selection of a sarcomere under brightfield. (C) Sarcomere diagram aligned to profiles. (D) Profiles of A and B.

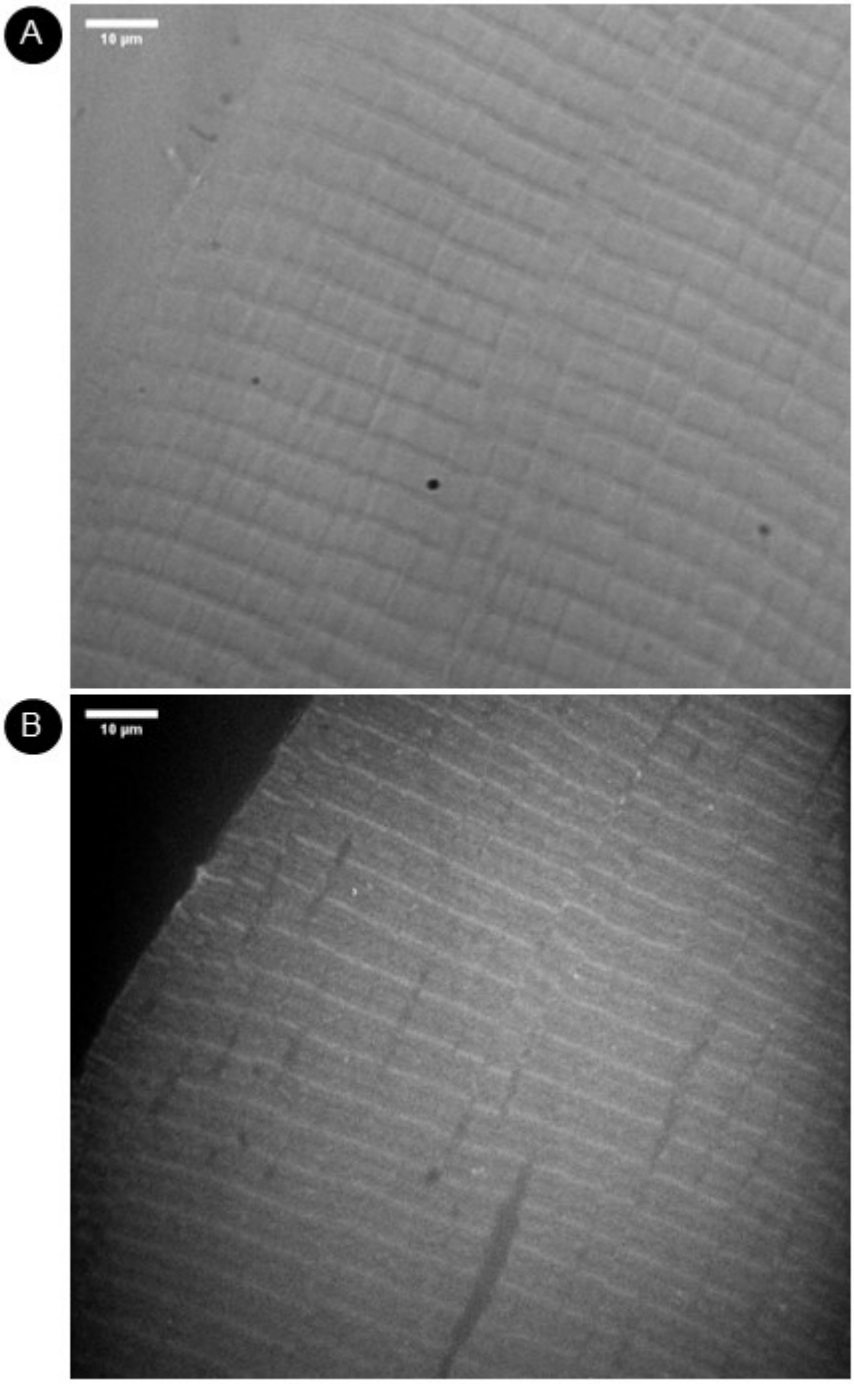

Figure 3.6-2. Expanded Myofibrils Immunolabeled for Myosin

Myofibrils expanded ~3.2x under brightfield (A) and with MF30 antibody (B). Scale is actual, not adjusted for expansion.

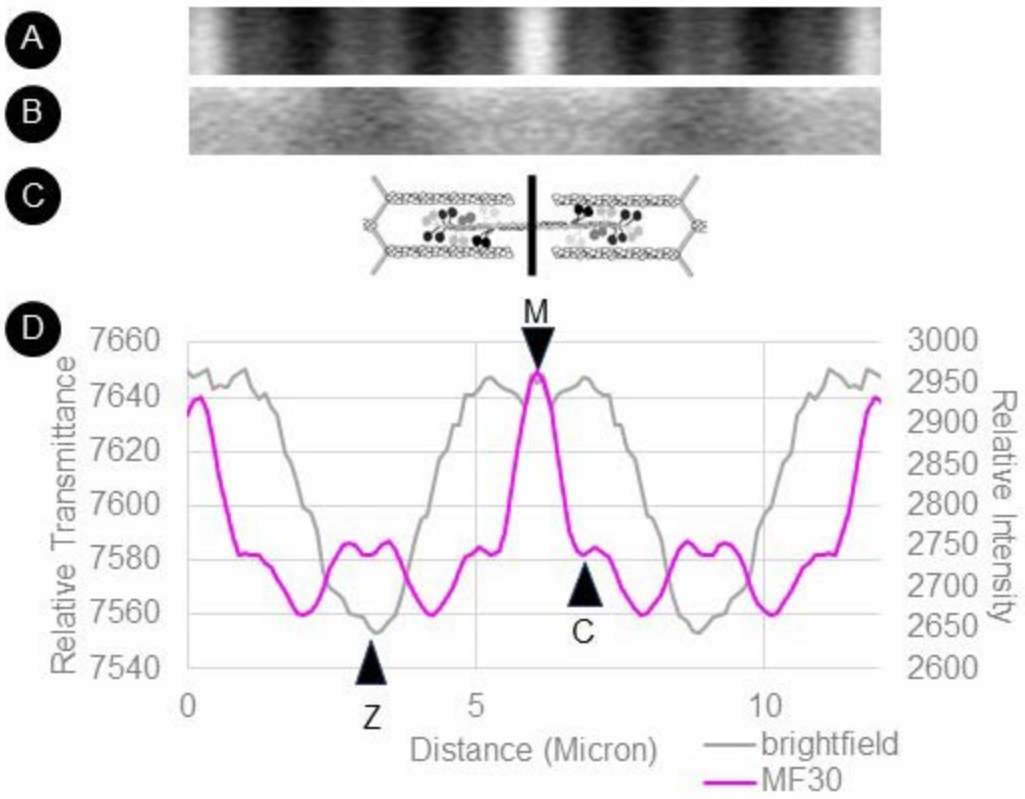

Figure 3.6-3. Myosin Immunolabeling Profile of the Expanded Sarcomere

Average sarcomere expanded ~3.2x labeled with MF30 antibody against myosin S2 (A) and under brightfield microscopy (B) aligned with sarcomere diagram (C). (D) Profiles of images A and B. “M” indicates the M-line, “Z” indicates the Z-disc, and “C” indicates a possible C zone.

Tropomyosin antibody labeling localized the thin filament and complemented the location of the thick filament as shown by myosin labeling and as predicted (Figures 3.6-4 and 3.6-5). The strongest fluorescent signal was found within the I band, the area of the sarcomere lacking myosin. Weaker fluorescent signal persisted into the A band as seen under brightfield, where the thin and thick filaments overlap, and a distinct lack of signal was observed at the Z-discs (Figure 3.6-5).

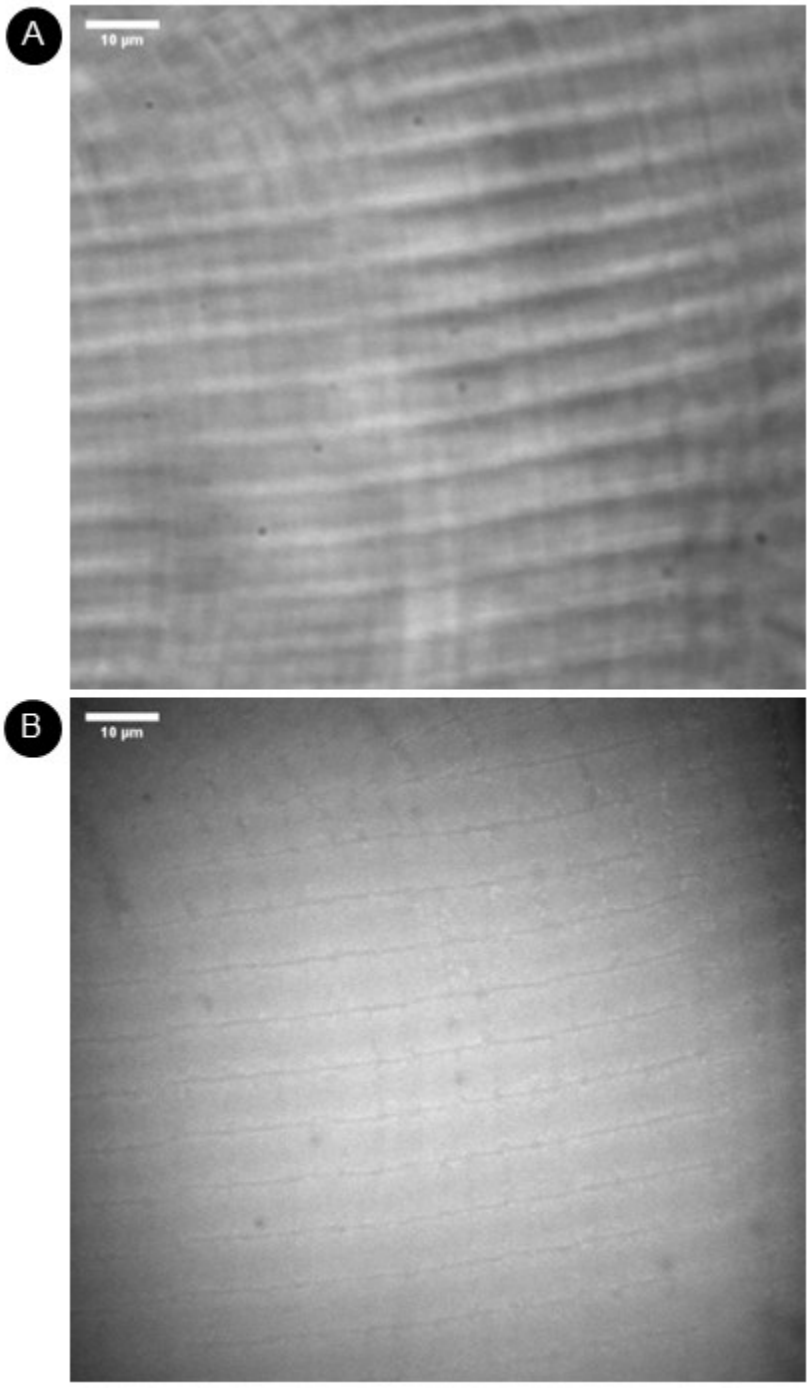

Figure 3.6-4. Expanded Myofibrils Immunolabeled for Tropomyosin

Myofibrils expanded ~3.9x under brightfield (A) and with CH1 antibody (B). Scale is actual, not adjusted for expansion.

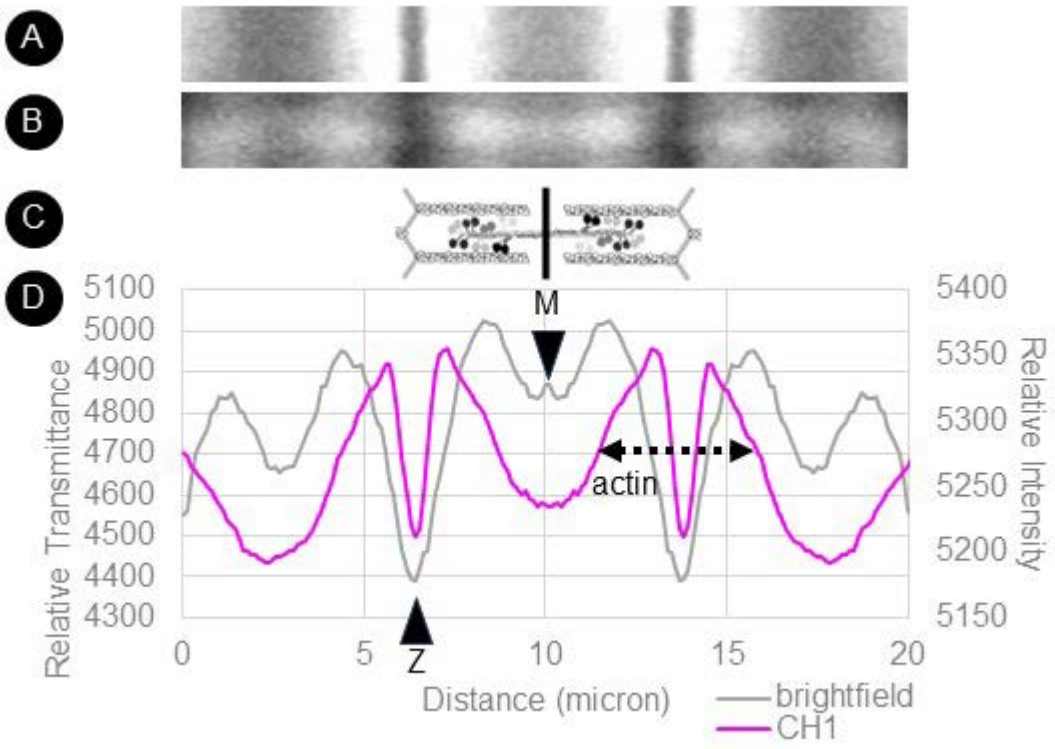

Figure 3.6-5. Tropomyosin Immunolabeling Profile of the Expanded Sarcomere (A) Average sarcomere expanded ~3.9x labeled with CH1 antibody against tropomyosin. (B) Single selection of a sarcomere under brightfield microscopy. (C) Sarcomere diagram aligned to profiles. (D) Profiles of images A and B. “M” indicates the M-line, “Z” indicates the Z-disc, and the double-headed arrow indicates the actin thin filament.

Similar experiments were attempted to localize the M-line protein myomesin, Z-disc protein alpha-actinin, and C-zone protein myosin-binding protein C. However, the antibodies used did not provide a signal beyond or distinct from autofluorescence. This was likely due to the relatively small abundance of these proteins in the sarcomere,

steric hinderances to crosslinking and to antibody binding in these highly crowded areas, and the intense dilution of fluorescence signal upon digestion and expansion.

3.7 Applying Transmitted Light Expansion Microscopy for Localizing Peptides

One major, immediate application of imaging expanded samples with transmitted light is to assist in the localization of fluorescently-tagged biomolecules within a sub-cellular context. This application was tested on a peptide designed to interact strongly with tropomyosin and fluorescently tagged on the N-terminus, called the “anti-tropomyosin peptide.” This peptide has been tested for its affinity to tropomyosin (Oloyede & Root, 2020) but has not been extensively characterized.

The anti-tropomyosin peptide’s interactions within the sarcomere resulted in distinct and detailed striations of fluorescent signal, indicating that the peptide’s binding is specific to some component of the sarcomere (Figure 3.7-1). Though not identical, the peptide showed a similar striation pattern to that of the anti-tropomyosin antibody (Figure 3.6-5), with the strongest fluorescent signal observed at the I band and a gap in signal at the Z-disc (Figure 3.7-2). Notably, transmitted light imaging helped identify the A band and the Z-disc without the use of antibodies or any other markers.

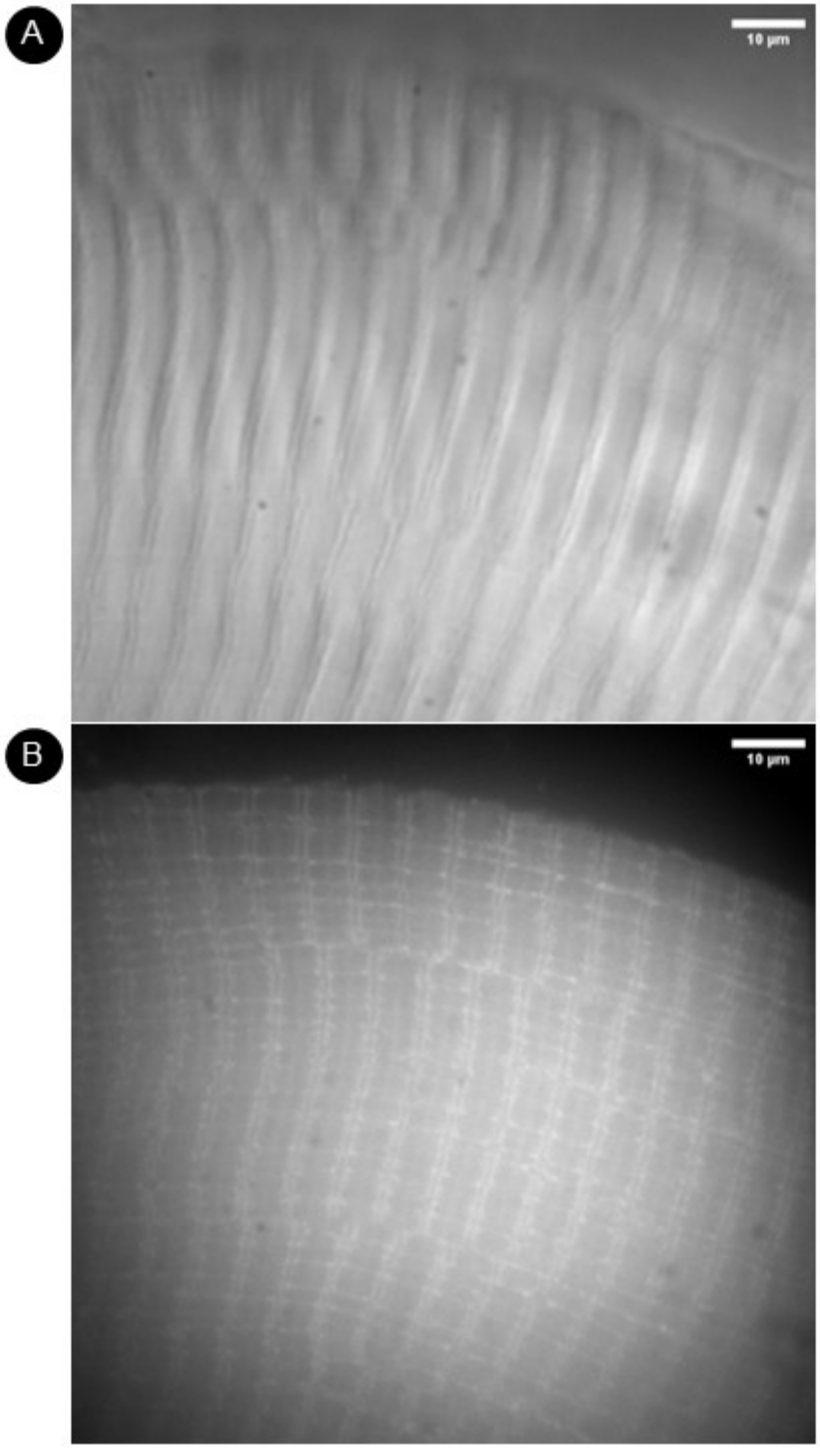

Figure 3.7-1. Expanded Myofibrils with Anti-tropomyosin Peptide

Myofibrils expanded ~2.9x under brightfield (A) and with TAMRA-anti-tropomyosin peptide (B). Scale is actual, not adjusted for expansion.

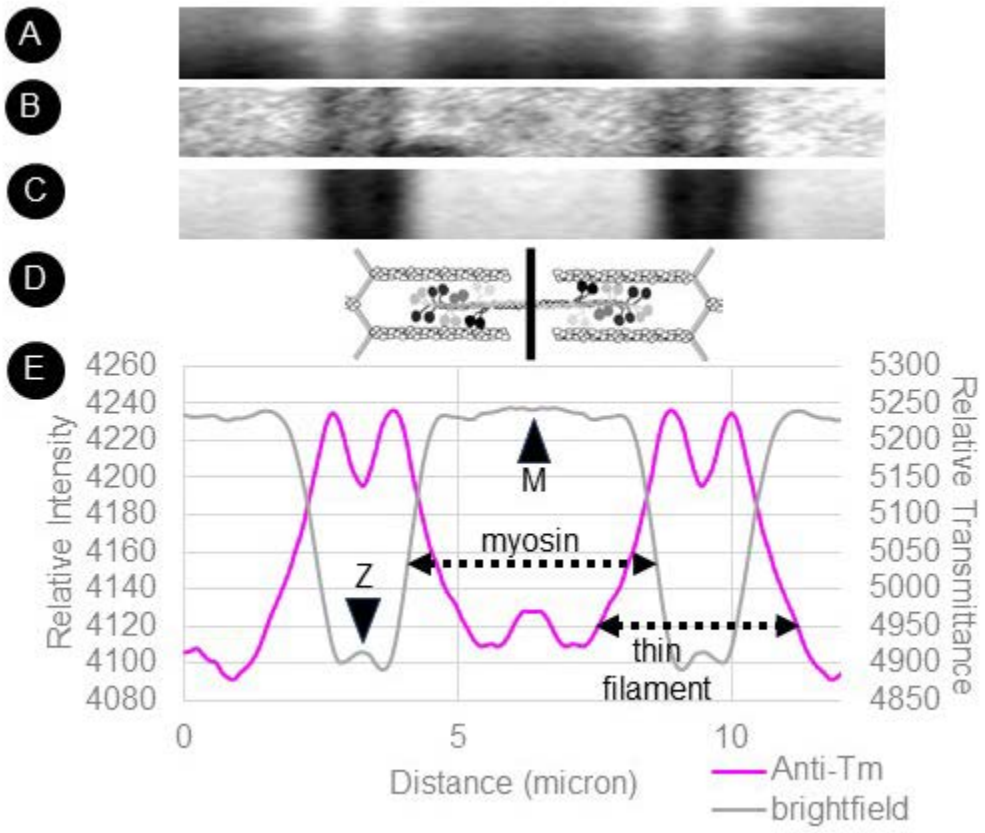

Figure 3.7-2. Anti-tropomyosin Peptide Profile of the Expanded Sarcomere

(A) Average fluorescence signal of anti-tropomyosin peptide in the sarcomere. (B) Single selection of a sarcomere under brightfield microscopy and (C) brightfield sarcomere average. (D) Profiles of images A and C. “M” indicates the M-line, “Z” indicates the Z-disc, and double-headed arrows indicate the actin thin filament and the myosin thick filament.

CHAPTER 4

DISCUSSION

4.1 Resolution of Transmitted Light Expansion Microscopy

Because ExM attains improved resolution without manipulating the optical path of the system used for imaging, its actual resolution can be no better than the ideal theoretical resolution of the system. However, ExM delivers an improvement in perceived resolution related to its expansion factor. For example, an imaging system with a resolution of 200 nm will still have an actual resolution of 200 nm as it images an expanded sample, but a perceived resolution of ~50 nm will be achieved if that sample is expanded 4x. Since the improvements in resolution are perceived and not actual, it is often more useful to assess this improvement by comparing the levels of detail visible in ExM-prepared samples and unprepared ones.

In myofibrils which have not been prepared for ExM, the I and A bands are all that can be distinguished. With expansions between 2-4x, the Z-disc becomes apparent within the I band under brightfield microscopy. The Z-disc varies in width from 30-50 nm in fast twitch skeletal muscle (Luther et al., 2003), so expansion improves perceived resolution to at least 50 nm in brightfield. Ultrastructure within the A band becomes apparent also, most notably a shadow aligned at the M-line useful for aligning sarcomeres for averaging.

4.2 The Contrast Problem

The major shortcoming of transmitted light ExM comes in the form of dramatically decreased optical contrast. Unlike fluorescence images of the same field of view,

images captured using brightfield or DIC require extensive adjustments to brightness and contrast to make the details of the image visible. Often, these images are captured "blind," since it is difficult to see areas of interest using the microscope's eyepiece.

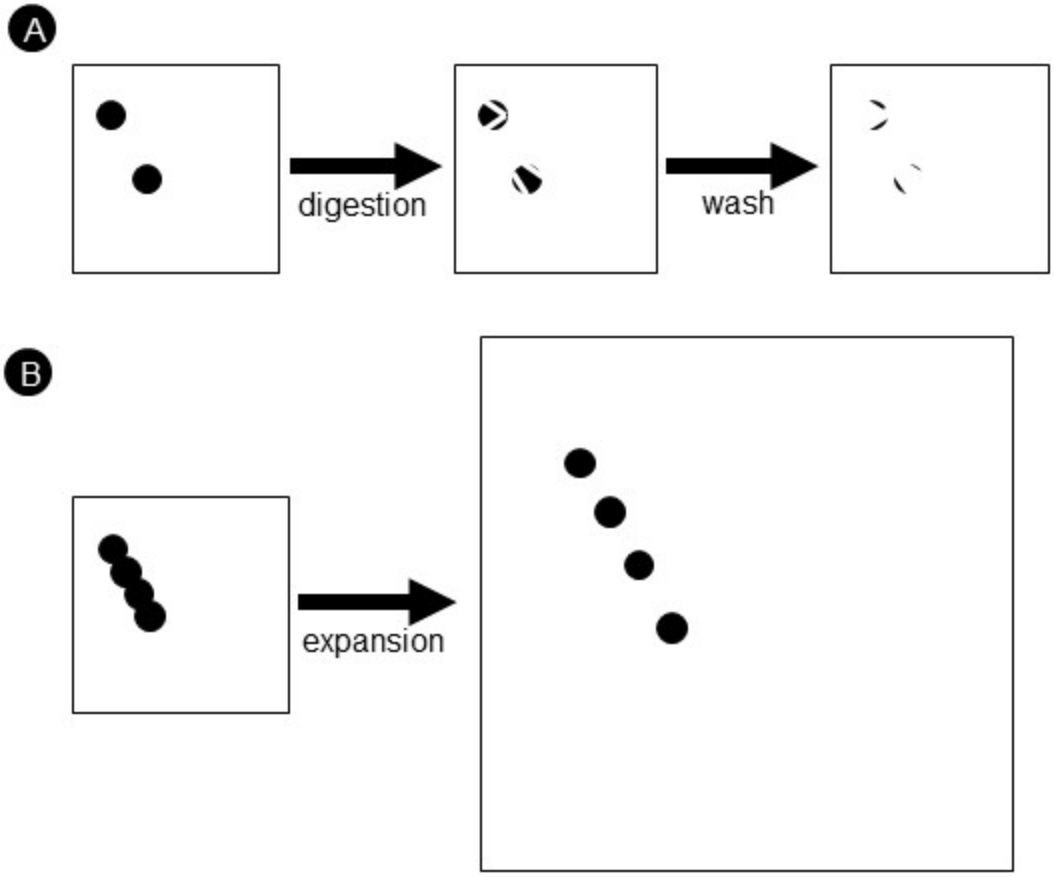

Figure 4.2-1. Mechanisms for Signal Dilution in Expansion Microscopy
(A) Fragments that were not crosslinked to the hydrogel are lost by washing after digestion. (B) Fluorescence signal is diluted upon expansion.

The contrast problem is expected in ExM for two reasons: digestion and dilution. ExM preparation requires the digestion of the sample in order to facilitate later expansion. Biomolecule fragments not crosslinked to the hydrogel are washed away

after digestion, resulting in a loss of material (Figure 4.2-1A). Upon expansion, fragments are pulled away from each other and the signal of a given object is diluted (Figure 4.2-1B). The method that increases resolution, in turn, decreases signal density.

All ExM methods face the consequences of digestion and dilution, and this is seen most clearly in the loss of fluorescence intensity after expansion. This is an active area of improvement that many of the newer variations on ExM have focused on, from post-expansion antibody labeling (Zwettler et al., 2020) to using molecular anchors (Shi et al., 2021). Digestion and dilution led to the expectation that nothing would be visible under transmitted light after expansion in the first place. To see anything at all was an unexpected discovery.

Since contrast under brightfield seems to be only weakly correlated with expansion factor, I hypothesize that loss of transmitted light contrast in ExM can be primarily attributed to digestion rather than signal dilution.

4.3 Contrast Generation in Transmitted Light Expansion Microscopy

The generation of optical contrast in transmitted light microscopy, especially in samples that do not absorb much light, heavily depends on light scattering and changes in light phase (see Introduction, section 1.2). In expanded samples, scattering could occur as the incident light interacts with the hydrogel matrix in addition to the sample itself. Therefore, contrast generation in transmitted light imaging of expanded samples could be achieved by two possible mechanisms: preservation of material through expansion, and the imprinting of hydrogel.

If contrast is generated from preserved material, one is seeing the remains of the digested sample itself when looking at an expanded sample in transmitted light. Light is primarily scattered by interacting with that material. This mechanism would require that protein or other material be crosslinked to the hydrogel and that digestion be stopped before all material is rendered invisible.

If contrast is generated from imprints in the hydrogel, one is not seeing the sample itself but the shape the hydrogel took around the sample during embedding. Here, light is primarily scattered by the hydrogel rather than any original material. Unlike the first mechanism, this one would not require any crosslinkers nor would it be possible to “over-digest” a sample. As long as the hydrogel monomers can permeate the sample thoroughly, they would polymerize into a shape surrounding sample. Once this shape is in place, the sample would no longer be needed at all.

It is known and accepted that some protein is preserved in the pro-ExM preparation. This is most clearly supported by the success of post-expansion antibody labeling approaches, which depend on antibody epitopes being both available and recognizable after both digestion and expansion (Zwettler et al., 2020). It was unclear whether enough protein is preserved through ExM to generate sufficient contrast in transmitted light microscopy but polarized light microscopy of expanded myofibrils suggests that there is not enough, especially for a mode such as brightfield. A band anisotropy was lost after expansion, indicating that the A band proteins which generate anisotropy were also lost. What is visible in an expanded sample not likely to be the sample itself, but evidence of the sample captured by the hydrogel.

In expanded mouse liver slices, as is often the case in unexpanded slices, the most identifiable features were the nuclei. Nuclear membranes contain a significant amount of protein which could be crosslinked to the hydrogel, but lipid components would not be crosslinked. Contrast generation dependent on preserved protein would reveal the most protein-dense features. However, if transmitted light contrast in expanded samples is attributable to imprints in the hydrogel, it can be expected that relatively large features such as the nuclei will make the most distinguishable impressions regardless of their protein density.

One variation of ExM, called “magnified analysis of the proteome,” or “MAP,” aims to prevent crosslinking between proteins in favor of crosslinking only with the hydrogel. Because proteins are not crosslinked to each other, protease digestion can be replaced with an SDS-based digestion which preserves more protein (Ku et al., 2016). With this approach, researchers have been able to apply generalized stains post-expansion, (Mao et al., 2020) and even combine ExM preparation with mass spectrometry imaging for a spatially-resolved proteomics study (Drelich et al., 2021). If enough protein is retained for reliable detection by mass spectrometry, perhaps it could also be enough to generate additional contrast in transmitted light microscopy modes.

4.4 Staining Post-Expansion

Achieving adequate contrast is a historical challenge for transmitted light microscopy since much of a cell is colorless (Goodwin, 2015). The use of stains has largely mitigated the contrast challenge in many fields and may help in the case of expanded samples also. Fluorescently-tagged antibodies and DAPI have been used

successfully post-expansion (Gaudreau-Lapierre et al., 2021; Zwettler et al., 2020), but a colorimetric equivalent has not yet been identified.

The immunohistochemical (IHC) staining attempted was not compatible with ExM. Staining was found to be largely arbitrary in expanded samples despite being specific, at least to the myofibril, when attempted independently from expansion. It is expected that post-expansion antibody labeling will only be successful to the degree that the antibody epitopes have been preserved. Polarized light microscopy of expanded myofibrils revealed that minimal protein—the protein crosslinked to the hydrogel—is preserved through the ExM preparation process. It can be concluded that the secondary antibody used for immunohistochemical staining never bound to its antigen since there was little to no antigen present post-expansion. Unfortunately, alkaline phosphatase cannot withstand digestion in the solution used here and thus staining cannot be successful when applying the secondary antibody before crosslinking. It is possible that changes to the digestion solution, especially the choice of protease, could allow for better retention of certain epitopes. However, the specimen must still be digested thoroughly enough to facilitate later expansion.

Even assuming perfect antibody diffusion and binding, the resulting IHC stain is never bound to the sample or antibody they came from. As a result, the targeted stain does not remain in the area near its antibody but diffuses away and becomes non-specific. This was expected but is also seen experimentally (Figure 3.6-1).

It is worth noting that even without specificity, the presence of the stain seemed to increase observed contrast. It is likely that the stain produced by the secondary antibody's chromogenic enzyme pools in the more open areas of hydrogel—areas that

have formed around sample material during embedding and became pits when that material was digested and washed away. Thus, if allowed to diffuse properly, colorimetric reagents in general could highlight differences in hydrogel density and increase contrast even without specificity.

The less-than-promising results from IHC staining with expansion assist in identifying some requirements for an ExM-compatible colorimetric stain. Using an alkaline phosphatase-based IHC stain, expansion factors did not surpass 3x. Gels visibly shrunk from their maximum levels of expansion after the addition of substrate solution. An ExM-compatible stain will need to be able to diffuse through a hydrogel matrix and have a high water content to avoid too much shrinkage.

Unfortunately, the requirement for a consistent aqueous environment quickly narrows the pool of possible stains. For example, though hematoxylin is used with hydrated tissues, it must be differentiated by washing in acidic alcohol (Harris, 1900; Titford, 2009). This treatment may reverse expansion and re-expansion with water may still wash the stain away. Similarly, eosin is known to be washed away if the solution is too aqueous: a major problem for a sample embedded in hydrogel. Coomassie blue dye may be an option for increasing contrast in ExM since it is used frequently with acrylamide gels. Common Coomassie staining solutions containing organic solvents such as acetic acid and methanol would not complement the aqueous environment of a hydrogel, but it is possible to stain without them (Lawrence & Besir, 2009).

4.5 Applications of Transmitted Light Expansion Microscopy

Transmitted light imaging of ExM samples has a major application for the Root lab: localizing therapeutic peptides at high resolutions. These peptides are designed to interact with specific sarcomeric proteins, and successful localization is key to their function. In the past, myosin-binding peptides have been assessed by ExM via a fluorescent tag (Tanner et al., 2019). These experiments revealed that the myosin-binding peptide prefers certain subregions of the thick filament over others, evidenced by consistent patterns of fluorescent signal across the thick filament. Antibodies against other sarcomeric proteins were used to investigate these patterns and identify subregions of the A band such as the C-zone. Other biochemical and biophysical binding assays suggested high affinity for myosin (Aboonasrshiraz, 2020; Singh, 2017), but it would have been difficult to be certain these myosin-binding peptides were actually binding specifically to myosin rather than other areas of the sarcomere when applied to a whole myofibrillar bundle rather than purified protein.

Capturing images in transmitted light channels will complement the fluorescent data reporting peptide location in the sarcomere. A familiar picture of the sarcomere in transmitted light modes can easily differentiate between filaments and even provide a more detailed location information within subregions without requiring additional antibody labeling that may compete with peptide binding. Here, complementary transmitted light images assisted in localizing an anti-tropomyosin peptide within the sarcomere by revealing the A band and Z-disc. In the context of a sarcomere or myofibrillar bundle, this also facilitated the determination of expansion factor since the A band serves as an internal ruler.

The Root lab is by no means the only place where transmitted light ExM could be applied. Any sub-cellular localization study could benefit from this, and this is partially evidenced by how commonly transmitted light images are paired with fluorescence images apart from ExM. While it is true that other super-resolution methods can be used for sub-cellular localization fluorescence data, the accompanying transmitted light channels are far behind in resolution. ExM can provide a series of complementary images that are comparable in resolution, all using common biochemical reagents and equipment.

Detectable sub-cellular regions of interest can act as visual landmarks without the need for additional tags, stains or dyes as was demonstrated in section 3.06 for sarcomeric features within myofibrils. For example, nuclei were visible in liver slices under brightfield microscopy after expansion (section 3.01), which could facilitate studies in nuclear localization. Though nuclear stains like DAPI are simple enough to use, they are not compatible with super-resolution methods requiring very specific fluorophores and would not be helpful in methods limited to just one fluorophore. A transmitted light image with visible nuclei would solve this problem.

Where ExM is already the imaging method of choice, using transmitted light is an easy addition to an established workflow. With sufficient contrast, transmitted light can be used to locate regions of interest without photobleaching fluorescent tags. Since loss of fluorescence through sample preparation is ExM’s biggest shortcoming, this can be incredibly helpful on a practical level. Plus, it may provide some useful data.

4.6 Conclusions

Much more can be seen with transmitted light in ExM than was previously assumed. The A and I bands in myofibrils, along with some of their substructures, can be identified under brightfield microscopy after ExM preparation. Similarly, this approach facilitates observation of features such as nuclei in liver tissue slices. Polarized light microscopy of expanded myofibrils suggests that imprints in the hydrogel from embedded material facilitate the generation of contrast in transmitted light microscopy despite the loss of the majority of material during ExM preparation.

The resolution of these biological samples under brightfield surpassed the resolution before preparation for ExM as demonstrated by the increased level of detail relative to similar samples which were not prepared for ExM. Identification of these features was shown to be compatible with imaging fluorescent labels and useful for localizing them in subcellular contexts.

This work also found that improvements in resolution with ExM come at the price of optical contrast, and that contrast is unrelated to expansion factor. While certain dyes may still be candidates for improving contrast under transmitted light modes, antigens are not preserved enough to facilitate meaningful immunohistochemical staining.
In conclusion, imaging ExM-prepared samples with transmitted light microscopy modes may be the beginning of transmitted light super-resolution microscopy.

REFERENCE LIST

Abbe, E. (1873). Beiträge zur theorie des mikroskops und der mikroskopischen wahrnehmung. *Archiv Für Mikroskopische Anatomie*, *9*(1), 413–468. https://doi.org/10.1007/BF02956173

Aboonasrshiraz, N. (2020). *Impact of anti-S2 peptides on a variety of muscle myosin S2 isoforms and hypertrophic cardiomyopathy mutants revealed by fluorescence resonance energy transfer and gravitational force spectroscopy*. University of North Texas.

Allen, R., & David, G. (1969). The Zeiss-Nomarski differential interference equipment for transmitted-light microscopy. *Zeitschrift Fur Wissenschaftliche Mikroskopie Und Mikroskopische Technik*, *69*(4), 193–221.

Aronson, J. F. (1967). Polarized light observations on a striated muscle contraction in a mite. *Journal of Cell Biology*, *32*, 169–179.

Bennett, P., Craig, R., Starr, R., & Offer, G. (1986). The ultrastructural location of C-protein, X-protein and H-protein in rabbit muscle. *Journal of Muscle Research and Cell Motility*, *7*(6), 550–567. https://doi.org/10.1007/BF01753571

Betzig, E., Patterson, G. H., Sougrat, R., Lindwasser, O. W., Olenych, S., Bonifacino, J. S., Davidson, M. W., Lippincott-Schwartz, J., & Hess, H. F. (2006). Imaging intracellular fluorescent proteins at nanometer resolution. *Science*, *313*(5793), 1642–1645. https://doi.org/10.1126/SCIENCE.1127344/SUPPL_FILE/BETZIG.SOM.PDF

Brown, J. H., & Cohen, C. (2005). Regulation of muscle contraction by tropomyosin and troponin: how structure illuminates function. *Advances in Protein Chemistry*, *71*, 121–159. https://doi.org/10.1016/S0065-3233(04)71004-9

Chang, J. B., Chen, F., Yoon, Y. G., Jung, E. E., Babcock, H., Kang, J. S., Asano, S., Suk, H. J., Pak, N., Tillberg, P. W., Wassie, A. T., Cai, D., & Boyden, E. S. (2017). Iterative expansion microscopy. *Nature Methods*, *14*(6), 593–599. https://doi.org/10.1038/NMETH.4261

Chen, F., Tillberg, P. W., & Boyden, E. S. (2015). Expansion microscopy. *Science*, *347*(6221), 543–548. https://doi.org/10.1126/SCIENCE.1260088

Coico, R. (2006). Gram staining. *Current Protocols in Microbiology*, *00*(1), A.3C.1-A.3C.2. https://doi.org/10.1002/9780471729259.MCA03CS00

Drelich, L., Aboulouard, S., Franck, J., Salzet, M., Fournier, I., & Wisztorski, M. (2021). Toward high spatially resolved proteomics using expansion microscopy. *Analytical Chemistry*, *93*(36), 12195–12203. https://doi.org/10.1021/ACS.ANALCHEM.0C05372

Fischer, A. H., Jacobson, K. A., Rose, J., & Zeller, R. (2008). Hematoxylin and eosin staining of tissue and cell sections. *Cold Spring Harbor Protocols*, *2008*(5), pdb.prot4986. https://doi.org/10.1101/PDB.PROT4986

Gao, M., Maraspini, R., Beutel, O., Zehtabian, A., Eickholt, B., Honigmann, A., & Ewers, H. (2018). Expansion stimulated emission depletion microscopy (ExSTED). *ACS Nano*, *12*(5), 4178–4185. https://doi.org/10.1021/ACSNANO.8B00776

Gaudreau-Lapierre, A., Mulatz, K., Béïque, J.-C., & Trinkle-Mulcahy, L. (2021). Expansion microscopy-based imaging of nuclear structures in cultured cells. *STAR Protocols*, *2*(3), 100630. https://doi.org/10.1016/J.XPRO.2021.100630

Goodwin, P. C. (2015). A primer on the fundamental principles of light microscopy: optimizing magnification, resolution, and contrast. *Molecular Reproduction and Development*, *82*(7–8), 502–507. https://doi.org/10.1002/MRD.22385

Gustafsson, M. G. L. (2000). Surpassing the lateral resolution limit by a factor of two using structured illumination microscopy. *Journal of Microscopy*, *198*(2), 82–87. https://doi.org/10.1046/J.1365-2818.2000.00710.X

Harris, H. (1900). On the rapid conversion of haematoxylin into haematein in staining reactions. *Journal of Applied Microscopic Laboratory Methods*, *3*(3), 777.

Heilemann, M., Van De Linde, S., Schüttpelz, M., Kasper, R., Seefeldt, B., Mukherjee, A., Tinnefeld, P., & Sauer, M. (2008). Subdiffraction-resolution fluorescence imaging with conventional fluorescent probes. *Angewandte Chemie International Edition*, *47*(33), 6172–6176. https://doi.org/10.1002/ANIE.200802376

Heling, L. W. H. J., Geeves, M. A., & Kad, N. M. (2020). MyBP-C: one protein to govern them all. *Journal of Muscle Research and Cell Motility*, *41*(1), 91–101. https://doi.org/10.1007/S10974-019-09567-1

Huxley, A. F., & Niedergerke, R. (1954). Structural changes in muscle during contraction: interference microscopy of living muscle fibres. *Nature*, *173*(4412), 971–973. https://doi.org/10.1038/173971a0

Huxley, H. E. (1969). The mechanism of muscular contraction. *Science*, 164(3886), 1356–1366. https://doi.org/10.1126/science.164.3886.1356

Huxley, H., & Hanson, J. (1954). Changes in the cross-striations of muscle during contraction and stretch and their structural interpretation. *Nature*, *173*(4412), 973–976. https://doi.org/10.1038/173973a0

Ito, M., Okamoto, R., Ito, H., Zhe, Y., & Dohi, K. (2021). Regulation of myosin light-chain phosphorylation and its roles in cardiovascular physiology and pathophysiology. *Hypertension Research*, *45*(1), 40–52. https://doi.org/10.1038/s41440-021-00733-y

Jungmann, R., Avendaño, M. S., Woehrstein, J. B., Dai, M., Shih, W. M., & Yin, P. (2014). Multiplexed 3D cellular super-resolution imaging with DNA-PAINT and Exchange-PAINT. *Nature Methods*, *11*(3), 313–318. https://doi.org/10.1038/nmeth.2835

Ku, T., Swaney, J., Park, J. Y., Albanese, A., Murray, E., Hun Cho, J., Park, Y. G., Mangena, V., Chen, J., & Chung, K. (2016). Multiplexed and scalable super-resolution imaging of three-dimensional protein localization in size-adjustable tissues. *Nature Biotechnology*, *34*(9), 973–981. https://doi.org/10.1038/nbt.3641

Lange, S., Himmel, M., Auerbach, D., Agarkova, I., Hayess, K., Fürst, D. O., Perriard, J. C., & Ehler, E. (2005). Dimerisation of myomesin: implications for the structure of the sarcomeric M-band. *Journal of Molecular Biology*, *345*(2), 289–298. https://doi.org/10.1016/J.JMB.2004.10.040

Lawrence, A. M., & Besir, H. (2009). Staining of proteins in gels with Coomassie G-250 without organic solvent and acetic acid. *Journal of Visualized Experiments*, *30*. https://doi.org/10.3791/1350

Lichtman, J. W., & Conchello, J. A. (2005). Fluorescence microscopy. *Nature Methods*, *2*(12), 910–919. https://doi.org/10.1038/nmeth817

Luther, P. K., Padrón, R., Ritter, S., Craig, R., & Squire, J. M. (2003). Heterogeneity of Z-band structure within a single muscle sarcomere: Implications for sarcomere assembly. *Journal of Molecular Biology*, *332*(1), 161–169. https://doi.org/10.1016/S0022-2836(03)00883-0

Mao, C., Lee, M. Y., Jhan, J. R., Halpern, A. R., Woodworth, M. A., Glaser, A. K., Chozinski, T. J., Shin, L., Pippin, J. W., Shankland, S. J., Liu, J. T. C., Liu, J. T. C., Liu, J. T. C., Vaughan, J. C., & Vaughan, J. C. (2020). Feature-rich covalent stains for super-resolution and cleared tissue fluorescence microscopy. *Science Advances*, *6*(22), 4542–4569. https://doi.org/10.1126/SCIADV.ABA4542/SUPPL_FILE/ABA4542_SM.PDF

Oloyede, B. I., & Root, D. D. (2020). Binding site analysis of an anti-tropomyosin destabilizing peptide using fluorescence microscopy and spectroscopy. *Biophysical Journal*, *118*(3), 276a-277a. https://doi.org/10.1016/j.bpj.2019.11.1586

Paul, D. M., Morris, E. P., Kensler, R. W., & Squire, J. M. (2009). Structure and orientation of troponin in the thin filament. *The Journal of Biological Chemistry*, *284*(22), 15007. https://doi.org/10.1074/JBC.M808615200

Quedan, D., & Root, D. D. (2022). Anti-S2 peptides and antibodies bind cooperatively to the myosin dimer with high affinity and stabilize the unfolded state of S2. *Biophysical Journal*, *121*(3), 517a. https://doi.org/10.1016/J.BPJ.2021.11.2725

Sahabandu, N., Kong, D., Magidson, V., Nanjundappa, R., Sullenberger, C., Mahjoub, M. R., & Loncarek, J. (2019). Expansion microscopy for the analysis of centrioles and cilia. *Journal of Microscopy*, *276*(3), 145–159. https://doi.org/10.1111/JMI.12841

Schindelin, J., Arganda-Carreras, I., Frise, E., Kaynig, V., Longair, M., Pietzsch, T., Preibisch, S., Rueden, C., Saalfeld, S., Schmid, B., Tinevez, J. Y., White, D. J., Hartenstein, V., Eliceiri, K., Tomancak, P., & Cardona, A. (2012). Fiji: an open-source platform for biological-image analysis. *Nature Methods 2012 9:7*, *9*(7), 676–682. https://doi.org/10.1038/nmeth.2019

Schmid, M., & Toepfer, C. N. (2021). Cardiac myosin super relaxation (SRX): a perspective on fundamental biology, human disease and therapeutics. *Biology Open*, *10*(2). https://doi.org/10.1242/BIO.057646/237268

Shi, X., Li, Q., Dai, Z., Tran, A. A., Feng, S., Ramirez, A. D., Lin, Z., Wang, X., Chow, T. T., Chen, J., Kumar, D., McColloch, A. R., Reiter, J. F., Huang, E. J., Seiple, I. B., & Huang, B. (2021). Label-retention expansion microscopy. *Journal of Cell Biology*, *220*(9). https://doi.org/10.1083/JCB.202105067/212454

Singh, R. R. (2017). *Stability of myosin subfragment-2 modulates the force produced by acto-myosin interaction of striated muscle*. University of North Texas.

Takahashi, K., & Hattori, A. (1989). α-actinin is a component of the Z-filament, a structural backbone of skeletal muscle Z-disks. *Journal of Biochemistry*, *105*(4), 529–536. https://doi.org/10.1093/oxfordjournals.jbchem.a122701

Tanner, B., Campbell, K., Qadan, M., Aboonasrshiraz, N., Quedan, D., Awinda, P., Bernardino-Shaefer, A., & Root, D. (2019). Anti-S2 peptides modulate myosin coiled coil structure and shift force-pCa curves in human cardiac muscle. *Biophysical Journal*, *116*, 263a. https://doi.org/10.1016/j.bpj.2018.11.1430

Tillberg, P. W., Chen, F., Piatkevich, K. D., Zhao, Y., Yu, C. C., English, B. P., Gao, L., Martorell, A., Suk, H. J., Yoshida, F., Degennaro, E. M., Roossien, D. H., Gong, G., Seneviratne, U., Tannenbaum, S. R., Desimone, R., Cai, D., & Boyden, E. S. (2016). Protein-retention expansion microscopy of cells and tissues labeled using standard fluorescent proteins and antibodies. *Nature Biotechnology*, *34*(9), 987–992. https://doi.org/10.1038/nbt.3625

Titford, M. (2009). The long history of hematoxylin. *Biotechnic and Histochemistry, 80*(2), 73–78. https://doi.org/10.1080/10520290500138372

Valli, J., Garcia-Burgos, A., Rooney, L. M., Vale de Melo Oliveira, B., Duncan, R. R., & Rickman, C. (2021). Seeing beyond the limit: a guide to choosing the right super-resolution microscopy technique. *Journal of Biological Chemistry*, 297(1), 1-13. https://doi.org/10.1016/j.jbc.2021.100791

Wichmann, J., & Hell, S. W. (1994). Breaking the diffraction resolution limit by stimulated emission: stimulated-emission-depletion fluorescence microscopy. *Optics Letters*, *19*(11), 780–782. https://doi.org/10.1364/OL.19.000780

Yu, C. C., Barry, N. C., Wassie, A. T., Sinha, A., Bhattacharya, A., Asano, S., Zhang, C., Chen, F., Hobert, O., Goodman, M. B., Haspel, G., & Boyden, E. S. (2020). Expansion microscopy of C. Elegans. ELife, 9, 1–78. https://doi.org/10.7554/ELIFE.46249

Zernike, F. (1935). Das phasenkontrastverfahren bei der mikroskopischen beobachtung. *Physik. Zeitschr.*, *36*, 848–851. https://cir.nii.ac.jp/crid/1570291225265809536.bib?lang=en

Zwettler, F. U., Reinhard, S., Gambarotto, D., Bell, T. D. M., Hamel, V., Guichard, P., & Sauer, M. (2020). Molecular resolution imaging by post-labeling expansion single-molecule localization microscopy (Ex-SMLM). *Nature Communications*, *11*(1), 1–11. https://doi.org/10.1038/s41467-020-17086-8